# Composite Activated Carbon from *Canarium schweinfurthii*/Polyethylene Terephthalate: Adsorption Test of Rhodamine B Dye Removal in Aqueous Solution

**Gadjui Youatou Boris[1], Ankoro Naphtali Odogu[2], Lekene Ngouateu René Blaise[1], Kouotou Daouda[1], Ndi Julius Nsami[1*], Ngomo Horace Manga[1], Ketcha Joseph Mbadcam[1]**

[1]Applied Physical and Analytical Chemistry Laboratory, Department of Inorganic Chemistry, Faculty of Science, University of Yaoundé I, Yaoundé, Cameroon
[2]Department of Chemistry, Faculty of Science, University of Buea, Buea, Cameroon
Email: leonelgadjui@gmail.com, a.naphtali@yahoo.com, *biegpielo2002@yahoo.com, kouotoudaouda@gmail.com, lekeneblaise@yahoo.fr, ngomo43@yahoo.co.uk, jketcha@yahoo.com

## Abstract

The present work deals on one hand with the valorization of wastes plastics, polyethylene terephthalate (PET) and *Canarium schweinfurthii* (CS) for the preparation of polyethylene terephthalate activated carbon (PETAC) and *Canarium schweinfurthii*/polyethylene terephthalate activated carbon (CS/PETAC). These adsorbents, on the other hand, were used for removal Rhodamine B (RhB) in an aqueous solution. PET and CS precursors were subjected to thermogravimetric analysis (TGA) and differential scanning colorimetry (DSC). Meanwhile PETAC and CS/PETAC were characterized using scanning electron microscopy-energy dispersive spectrometry (SEM-EDS), X-ray fluorescence (XRF), Fourier transformed infrared spectroscopy (FT-IR) and nitrogen adsorption/desorption ($N_2$-BET). The $N_2$-BET results revealed an increase of the specific surface area from 6.75 $m^2/g$ to 1282.0 $m^2/g$ for PETAC and CS/PETAC. The results of characterization indicated the key role played by plastic wastes to enhance the structural and functional properties of CS/PETAC. The RhB removal from the aqueous solution onto PETAC and CS/PETAC was found to be independent of pH, with an optimal contact time of RhB removal within 10 min for materials. The non-linear adsorption isotherm data for the adsorption process showed that the Langmuir and Freundlich models best fitted the RhB adsorption onto PETAC meanwhile only the Freundlich adsorption isotherm gave the best fit for CS/PETAC according to the correlation coefficient value closed to unity. The pseudo-first and pseudo-second-order ki-

netic models best described the RhB dye removal on both adsorbents. Additionally, the Elovich model confirmed that chemisorption was the main mechanism followed. These findings proved that CS seeds and PET wastes are low-cost precursors that should be given an added value by transforming them into an outstanding carbon material for dye removal in liquid effluent.

## Keywords

## 1. Introduction

The discovery of plastic materials has changed human behavior from domestic to industrial levels. Plastic materials were reported to have tremendous benefits and advantages to mankind because they have highly influenced day-to-day life and people fail to think of easy life without the use of plastic materials. Plastics materials are considered as one of the widely used synthetic polymers around the world [1]. Although plastic materials are essential in human life, they are currently used in electronics, buildings and other industries [2]. The annual production of plastic materials has doubled over the past fifteen years to 245 million tons. This increased production of plastic waste has led to a big environmental disturbance that needs to be solved. Annually and due to their excessive usage, the plastic waste in billions of tons accumulates around the world [3]. Among the total solid wastes generated in the environment, the plastic waste topped the list [4]. It has been proved that, under natural conditions, the plastics materials are non-degradable organic matter, thus considered as a major environmental problem [5] [6] [7].

Recycling plastic waste is an alternative solution to producing new materials and limiting the mountains of trash that accumulate plastic waste and cause serious threats to the environment and wildlife [8]. Plastic wastes are considered the most hazardous solid waste [9]. In plastic waste dumping sites, terrestrial animals are used to feed from thrown-off foodstuff along with plastic carrier bags. In the past, the consumption of such foods along with plastic carrier bags led to the death of cows.

Among the various methods to reduce plastic waste colonization, the biodegradation technology is known to be the most accepted and eco-friendly method. The bioremediation method proceeds due to the potential microorganism action and without using any kind of heat [10]. Based on the oxygen utilization in the biodegradation technology of the toxic compounds (organic in nature), two types of biodegradation processes are recognized: That are the aerobic and anaerobic biodegradation [11]. Plastic wastes that end up in landfills break down aerobically into water and $CO_2$, whereas the plastic waste dumped at ex-situ level degrades anaerobically and lead to the generation of $H_2O$, $CO_2$ and $CH_4$ as end

products [10]. Different microbes are required to break down the polymers into water and $CO_2$ in a multistep process of aerobic biodegradation [12]. During aerobic biodegradation, some microbes lead to polymer breakdown into smaller components such as oligomers, dimers, and monomers and other microbes convert them into smaller end products and later consume these generated smaller components [8] [11].

Furthermore, during the last two decades, researchers have paid more attention on the development and tailoring of adsorbent materials for wastewater treatment purposes. The removal of heavy metals, dyes and pesticides from wastewater is essential in order to keep the environment clean and human health safe [13] [14] [15]. Besides the aforementioned pollutants, Rhodamine B dye is always incriminated in several environmental problems such as respiratory affection, cancer and eye irritation [16] [17]. For the RhB remediation in contaminated water, several methods including thermal degradation using non-thermic plasma, electrocoagulation, reverse osmosis and adsorption have been developed [18] [19] [20]. Also, [21] [22] [23] studied the Photodegradation of methyl orange and Rhodamine dye on $TiO_2$ $Fe_3O_4$@ZnO@graphene oxide nanocomposite. Due to the aromatic structure of dye organic pollutants, the application of some of the mentioned methods is not very effective in eliminating pollutants [24]. Among the above-cited methods, the adsorption technique is promising based on its economical aspect, flexibility, simplicity of design and ability to remove various pollutants even at low concentrations [25] [26].

From the literature, various adsorbents including carbon-based materials, chitosan, clay, volcanic pumice and zeolite have been successfully used for RhB dye removal [27]-[31]. For industrial water treatment, the activated carbons are so far considered as the best adsorbent due to their various type of surface functional groups, well-developed pore structure, high porosity and large surface area which make them to be called versatile materials [27] [32]. In general, activated carbons are considered to possess hydrophobic properties, which considerably reduce their adsorption capacities towards RhB from aqueous media [33] [34] [35]. In order to increase their adsorption capacities towards RhB, the activated carbon's surface can be modified by reinforcing them to form composite material [27] [36]. It has been reported from the literature that a composite can be made by either reinforcing the carbon skeleton/chains or its surface using biological, physical, or chemical methods [37] [38] [39].

Carbon composites are considered to be good materials with various applications in environmental protection. Their most found property is the increase of adsorption capacity towards some hazardous species. In Cameroon, the African black fruits (*Canarium schweinfurthii*) are abundant and available in large quantities. The *Canarium schweinfurthii* seeds have been successfully used to prepare activated carbon [40] [41], but there is not much work as far as our knowledge is concerned which deal with the production of carbon composite

materials based *Canarium schweinfurthii* seeds combined with PET wastes [42]. Hence, the aim of this work is to prepare a composite carbon material based *Canarium schweinfurthii* seeds and polyethylene terephthalate wastes and finally use non-linear consideration to study the equilibrium and kinetics adsorption of RhB dye selected as a representative of cationic basic dye since it is frequently found in industrial wastewater.

In our previous work, the linear least-square method was widely used by transforming the equation into a conventional linear form to calculate or predict the isotherms/kinetics parameters or the most fitted models of RhB dye adsorption [25] [30]. These models are principally subjected to their goodness of fit to the experimental data with the magnitude of the coefficient of determination that is close to unity [43]. Linear methods have been proven to have significant limitation related to the linearized form of isotherms/kinetics equations by producing a vast number of different outcomes, which implicitly alter the error structure, violates the error variance and normality assumptions of standard least squares leading to the bias of the adsorption data [25] [44] [45] [46]. Due to the inherent bias from linearization, the non-linear regression will be used in this work to provide a mathematically rigorous method for determining the isotherm/kinetic parameters using the original form of the equations [44] [45].

The aim of the present work was to valorise the local agricultural and plastics waste in the preparation of biocomposite applied to the removal of RhB from water. The adsorbents were characterized using various techniques including thermogravimetric analysis-differential scanning colorimetry (TGA-DSC), scanning electron microscopy-energy dispersive spectrometry (SEM-EDS), X-ray fluorescence (XRF), Fourier transformed infrared spectroscopy (FT-IR) and nitrogen adsorption/desorption ($N_2$-BET). The effect of pH, time, mass and initial concentration of RhB were investigated by performing batch adsorption experiments. The kinetics and isotherm studies were also investigated based on the adsorption results.

## 2. Materials and Methods

### 2.1. Sampling of Precursors and Preparation of Adsorbents

The PET bottles were collected from the water stream in the neighborhood of Oyomabang in the Yaoundé city capital of Cameroon. They were chopped in smaller sizes of about 0.6 - 1.0 cm in diameter and dried. The PET particles were then carbonized in a controlled Carbolite tube furnace (Carbolite 1200°C Tube Furnaces, Keison Products) at 300°C in order to obtain PET carbonized material without elastic properties. The non-elastic PET was ground and sieved to sizes of around 0.6 to 1.6 mm. 10 g of the non-elastic PET was mixed with phosphoric acid used as an activating agent, dried and the dry sample was once again carbonized in the Carbolite tube furnace at 300°C for 1.0 h and the resulting carbon material was called PETAC. The sampling of *Canarium schweinfurthii* seeds was

done in some markets in the West region of Cameroon. They were first washed abundantly with tap water to remove all dirties, followed by washing with distilled water and drying. The seeds were ground and sieved at the particle sizes ranging 1.0 - 2.0 mm. The sieved sample was mixed with phosphoric acid (orthophosphoric acid, 85% of purity from PA Panreac, used without any further purification) and the non-elastic PET in the ratio 1:1:1. The resulting mixture was stirred for 1.0 h and oven-dried for 24 h at 110˚C then allowed to cool in a desiccator and finally carbonized at 600˚C at the heating rate of 10˚C and the composite carbon material obtained was coded as CS/PETAC. However, the temperature of carbonization of PET to PETAC and the CS, PET and phosphoric acid mixture to CS/PETAC was obtained from TGA Analysis (**Figure 1** and **Figure 2**).
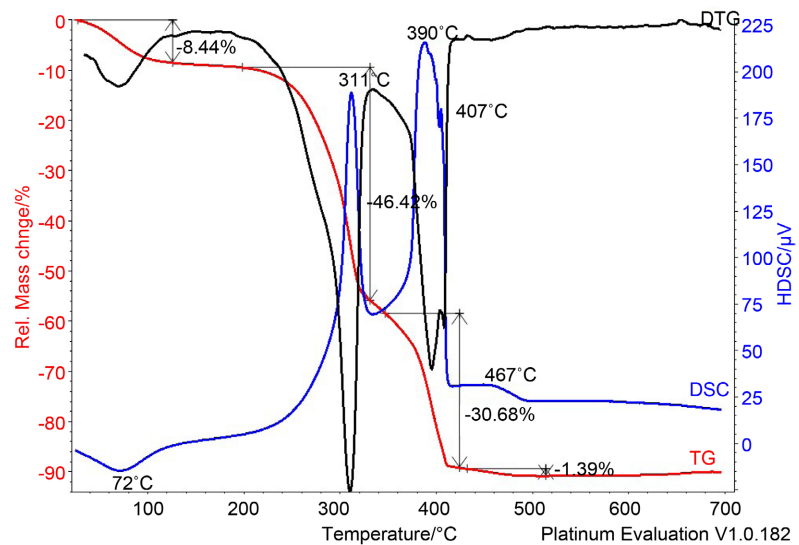


**Figure 1.** Representation of the thermogravimetric graph of CS.
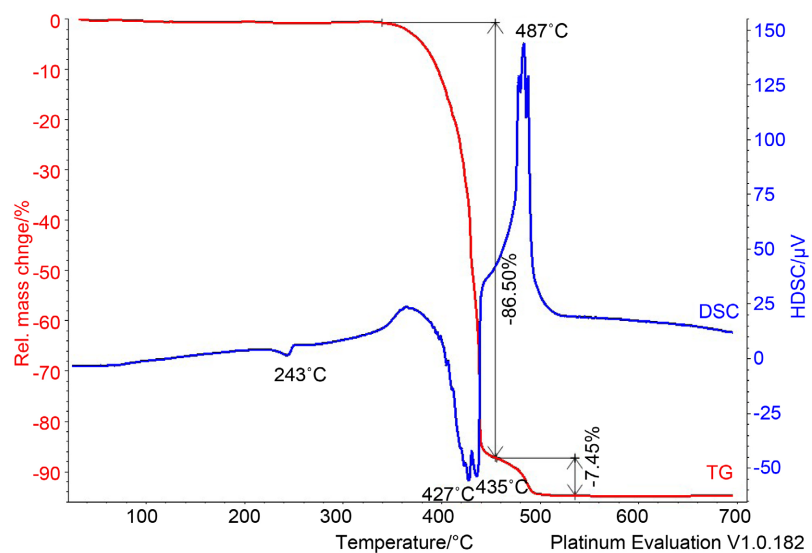


**Figure 2.** Representation of the thermogravimetric graph of PET.

## 2.2. Samples Characterization

The thermogravimetric analysis (TGA) and differential scanning calorimetry (DSC) of CSseeds and PET were evaluated using a thermogravimetric analyzer, TGA/DSC (LENSEIS STAPT-1000 thermal analyzer). The surface morphologies of PETAC and CS/PETAC materials were observed using a Scanning Electron Microscopy equipped with an Energy Dispersive Spectrometer (SEM/EDS, LEO 1455 VP). The X-ray fluorescence spectrometry (PANalytical X' Pert Pro) of CS, PET, PETAC and CS/PETAC were carried out. The FT-IR measurements were also carried out in the absorbance mode ranging from 400 to 4000 cm$^{-1}$ using Universal ATR, Crystal: Platinum, Diamond, Bounces: 1, and Solvent: ethanol for surface functional groups determination. The pore structure and surface area of the PETAC and CS/PETAC were done using nitrogen adsorption/desorption at −196°C, which was conducted using a gas sorption analyzer, Quantachrome, NOVA 1000 series, USA.

## 2.3. Batch Adsorption Experiments

Batch adsorption experiments were carried out by mechanical agitation at room temperature (27°C ± 0.1°C). For each run, 20.0 mL of RhB dye of known initial concentration was treated with a known mass of PETAC or CS/PETAC adsorbents. After agitation use Multipurpose Flask Shaker TT12F from Techmel and Techmel USA at 160 rpm for a fixed period. The solution was filtered using a 0.2 μm Millipore filter and the filtrate was subsequently analyzed for RhB residual concentration by UV/Vis spectrophotometer, model S23A from Techmel and Techmel USA at a wavelength of 660 nm. Similar measurements were also carried out for various PETAC and CS/PETAC doses (0.01 to 0.06 g), pH (2 to 10) and initial concentration of RhBsolution (50 to 100 mg/L). The RhB amount adsorbed per unit mass of adsorbent at equilibrium $Q_e$ (mg/g) was calculated by using the following expression.

$$Q_e = \frac{C_o - C_e}{m} \times V \tag{1}$$

$$Q_t = \frac{C_o - C_t}{m} \times V \tag{2}$$

where $C_o$, $C_e$ and $C_t$ (in mg/L) are the initial, equilibrium and concentration at the time, $t$, of RhB solution respectively, $m$ (g) the mass of adsorbent and $V$ (L) the volume of the solution.

## 2.4. Non-Linear Adsorption Isotherms and Kinetic Modeling of the Adsorption Data

### 2.4.1. Adsorption Isotherm Studies
Three non-linear adsorption isotherms: Langmuir, Freundlich and Temkin isotherms were used to analyze the experimental data and their non-linear forms [25] [45] [46] [47]. The respective isotherms equations models used are given below.

$$q_e = \frac{q_m K_L C_e}{1 + K_L C_e} \tag{3}$$

$$q_e = K_F C_e^{\frac{1}{n}} \tag{4}$$

$$q_e = \frac{RT}{b} \ln(K_T C_e) \tag{5}$$

where $C_e$ (mg/L) and $q_e$ (mg/g) are the concentration and the adsorbed quantity of RhB at equilibrium, $q_m$ is the maximum adsorbed quantity, $K_L$ (L·mg$^{-1}$) is the Langmuir adsorption constant, $K_F$ (L·mg$^{-1}$) is the Freundlich adsorption constant related to adsorption capacity, $n$ is the energetic heterogeneity of surface, $K_T$ is the equilibrium binding constant (L·mg$^{-1}$) corresponding to the maximum binding energy and constant $b$ (J/mol) is related to the heat of adsorption, $K$ (mol$^2$·k·J$^{-1}$) is a constant related to the adsorption energy. $R$ (8.314 J·mol$^{-1}$·K$^{-1}$) is the perfect gas constant and $T$ (K) is the temperature at which the adsorption took place.

### 2.4.2. Kinetics Studies

To describe the mechanism of the adsorption process and the rate-controlling step of RhB onto PETAC and CS/PETAC adsorbents, four kinetic models namely pseudo-first-order, pseudo-second-order, Elovich and intraparticle diffusion were used to correlate the experimental data and their non-linear forms [25] [45] [46] [47] [48]. The respective kinetics equations models used are given below.

$$q_t = q_e\left[1 - \exp(-k_1 t)\right] \tag{6}$$

$$q_t = \frac{q_e^2 k_2 t}{1 + q_e k_2 t} \tag{7}$$

$$q_t = \frac{1}{\beta}\ln(1 + \alpha\beta t) \tag{8}$$

$$q_t = k_i t^2 + C_i \tag{9}$$

where, $q_t$ and $q_e$ (mg/g) are the adsorbed quantity at a given time, $t$ and equilibrium respectively. $K_1$ (min$^{-1}$), $K_2$ (g·mg$^{-1}$·min$^{-1}$) and $k_{id}$ (mg·g$^{-1}$·min$^{-0.5}$) are the rate constants of pseudo-first-order, pseudo-second-order and intra-particle diffusion models respectively. $A$ (mg·g$^{-1}$·min$^{-1}$) is the rate of the initial adsorption, $\beta$ (g·mg$^{-1}$) is the desorption constant and $C_i$ is a constant value depicting the boundary layer effect.

The validity of the different aforementioned models was evaluated using correlation coefficient ($R^2$), root mean square error (*RMSE*) and Chi-square test ($\chi^2$) [45]. The respective relations are given below:

$$R^2 = 1 - \frac{\sum_{n=1}^{n}\left(q_{e.exp,n} - q_{e.pre,n}\right)^2}{\sum_{n=1}^{n}\left(q_{e.exp,n} - \overline{q_{e.exp,n}}\right)^2} \tag{10}$$

$$RMSE = \sqrt{\frac{\sum_{n=1}^{n}\left(q_{e.\exp,n} - q_{e.pre,n}\right)^2}{n-1}} \tag{11}$$

$$\chi^2 = \sum_{n=1}^{n} \frac{\left(q_{e.exp,n} - q_{e.pre,n}\right)^2}{q_{e.exp,n}} \tag{12}$$

where, $q_{e.exp}$ and $q_{e.pre}$ are experimental and predicted equilibrium adsorption capacities. The best fitting and similarity of a model with experimental data is decided by the largest value of $R^2$ or the smallest values of $RMSE$ and $\chi^2$.

## 3. Results and Discussion

### 3.1. TGA d DSC Results of CS and PET Precursors

The thermochemical behavior and the phenomena involved during the pyrolysis of CS and PET are recorded in **Figure 1** and **Figure 2** respectively.

**Figure 1** displays four thermal points. The first one appears at 72°C corresponding to the departure of free water at the surface of CS with a weight loss of approximately 8.44% which is an endothermic process. The second thermal point appears around 311°C resulting from a weight loss of about 46.42%, this weight loss could be attributed to the hemicellulose degradation with an exothermic phenomenon. The third thermal point appears around 390°C corresponding to a weight loss of 30.68%, this cellulose degradation is followed by the beginning of the lignin degradation. The fourth thermal point appears between 400°C and 520°C which corresponds to total lignin decomposition with a weight loss of 1.39%, this low value of weight loss may be due to the low level of lignin in CS precursor. These results are in agreement with the work done by Raveendran *et al.* 1995 who showed that cellulose decomposes in a narrow temperature range of 300°C - 400°C and 325°C - 375°C while lignin dissociated in a much wider temperature zone 250°C - 550°C and 200°C - 500°C [49]. These authors also indicated that hemicellulose which is the least thermally stable compound decomposes at low temperatures ranging 200°C - 250°C and above 520°C, there are bonds disruption thus allowing volatile matters departure. Only inorganic matter like ash remains, consequently the carbonization temperature of CS was chosen between 400°C and 600°C.

According to **Figure 2**, it is noticed two main thermal points. The first point thermal point occurs at 243°C and is an endothermic phenomenon that can be attributed to carbon skeleton rearrangement without breaking the bonds of the chemical structure of PET. The first weight loss of 86.50% is observed at 427°C indicating carbon-carbon skeletons destruction. The second weight loss appears at 487°C indicating the decarboxylation of the polymers precisely the carbon-oxygen bonds. Beyond 500°C, no further weight loss is observed, hence the PET was totally carbonized and only ash remains.

### 3.2. X-Ray Fluorescence Analysis Results

**Figure 3** shows the spectra of the results for the elemental composition of PET,
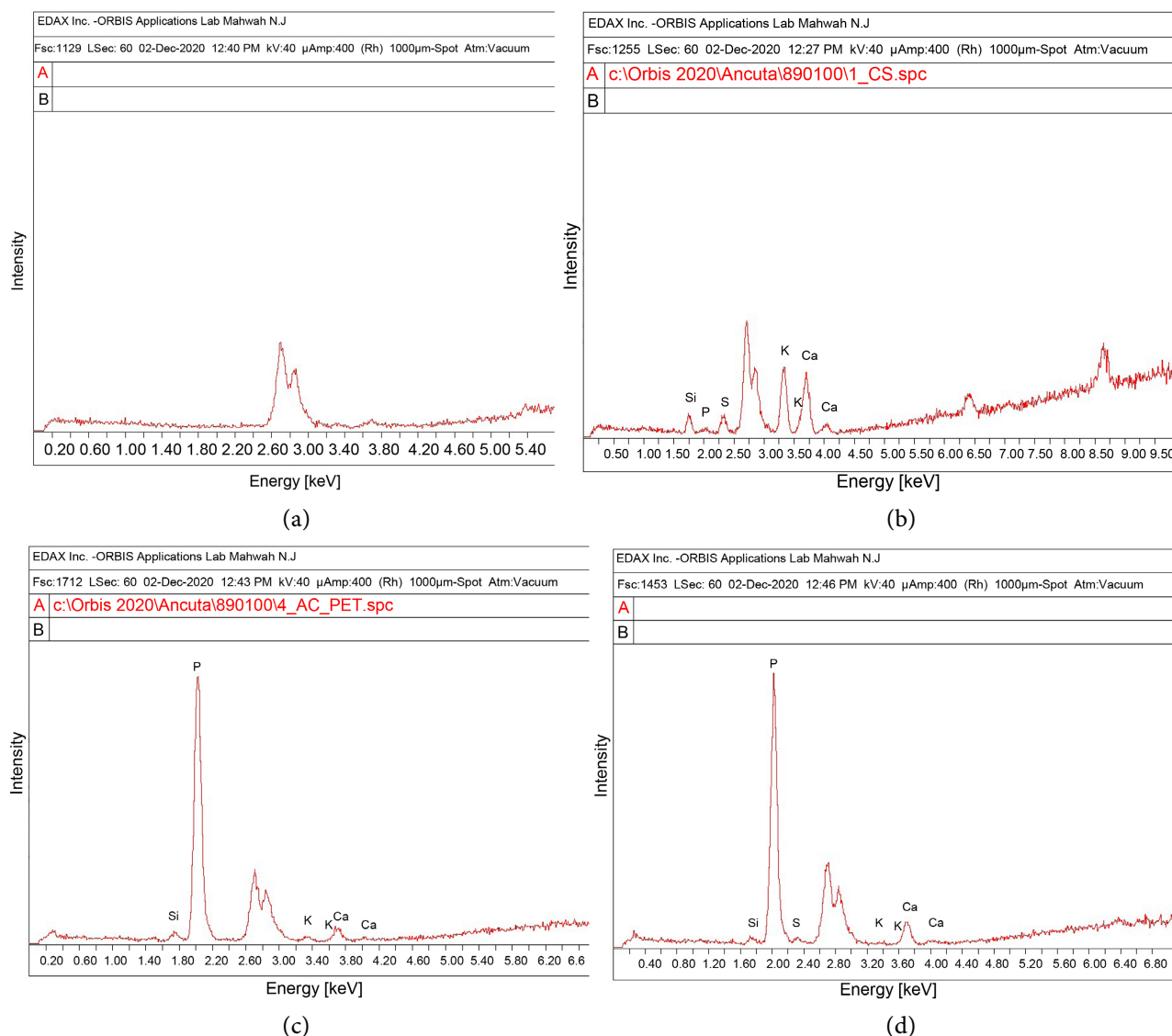
**Figure 3.** X-ray fluorescence Spectra of PET (a), CS (b), PETAC (c) and CS/PETAC (d).

CS, PETAC and CS/PETAC samples which are highlighted by the X-ray fluorescence analysis method.

According to **Figure 3**, the peaks appearing at 2.7 keV correspond to the existence of the metal Rh due to the characteristics of the spectrometer tube, *i.e.*, the fluorescence is caused by the material of the anode. Indeed, rhodium is used in some X-ray tubes, on their anodes, especially in the field of X-ray fluorescence spectrometry. Therefore, it should not be taken into account when interpreting the spectra of all materials. **Figure 3(a)** has no particular peaks other than those of rhodium indicating that the crude PET material contains only organic elements like carbon, hydrogen, oxygen… and no metallic elements. **Figure 3(b)** shows the *Canarium schweinfurthii* spectrum and according to that spectrum, the different elements found are potassium, calcium, sulfur, silicon and phosphorus. It is also observed that the major elements are potassium and calcium

while the other elements present are in trace. **Figure 3(c)** and **Figure 3(d)** corresponding to PETAC and CS/PETAC spectra respectively indicate calcium, sulfur, silicon, phosphorus and potassium presence with the phosphorus element in huge amounts and others in trace state. It can be noticed the absence of potassium element or its presence in trace in PETAC and CS/PETAC carbon materials may result in their activation with phosphoric acid. In that way, the potassium reacted with the phosphoric acid to form potassium phosphate which is soluble in water. This potassium phosphate was therefore leached out during the washing of the adsorbent, hence its absence or its presence in a very low concentration.

### 3.3. FT-IR Analysis Results

The FT-IR spectrum of PET is given in **Figure 4**.

It shows four main absorption bands at 2800 - 3000 cm$^{-1}$, 1500 - 1700 cm$^{-1}$, 1300 - 1400 cm$^{-1}$ and 1000 - 1200 cm$^{-1}$. The band located at 2989 cm$^{-1}$ is characteristic of the asymmetric and symmetric deformation and elongation valence vibrations of the $-CH_2=CH_3$ group. The band at 1713 cm$^{-1}$ may be due because of the elongation vibration of C=O in ketones, aldehydes, lactones, and carbonyl and aromatic rings. The band recorded between 1300 and 1401 cm$^{-1}$ is attributed to the deformation and elongation vibrations of C=C bonds of aromatic rings. The bands observed at 1000 cm$^{-1}$ and 1200 cm$^{-1}$ are the consequence of the C-O elongation vibration in esters. For the bands located at 900 and 400 cm$^{-1}$, they are attributed to the out-of-plane deformation vibration of aromatic C-H bonds.
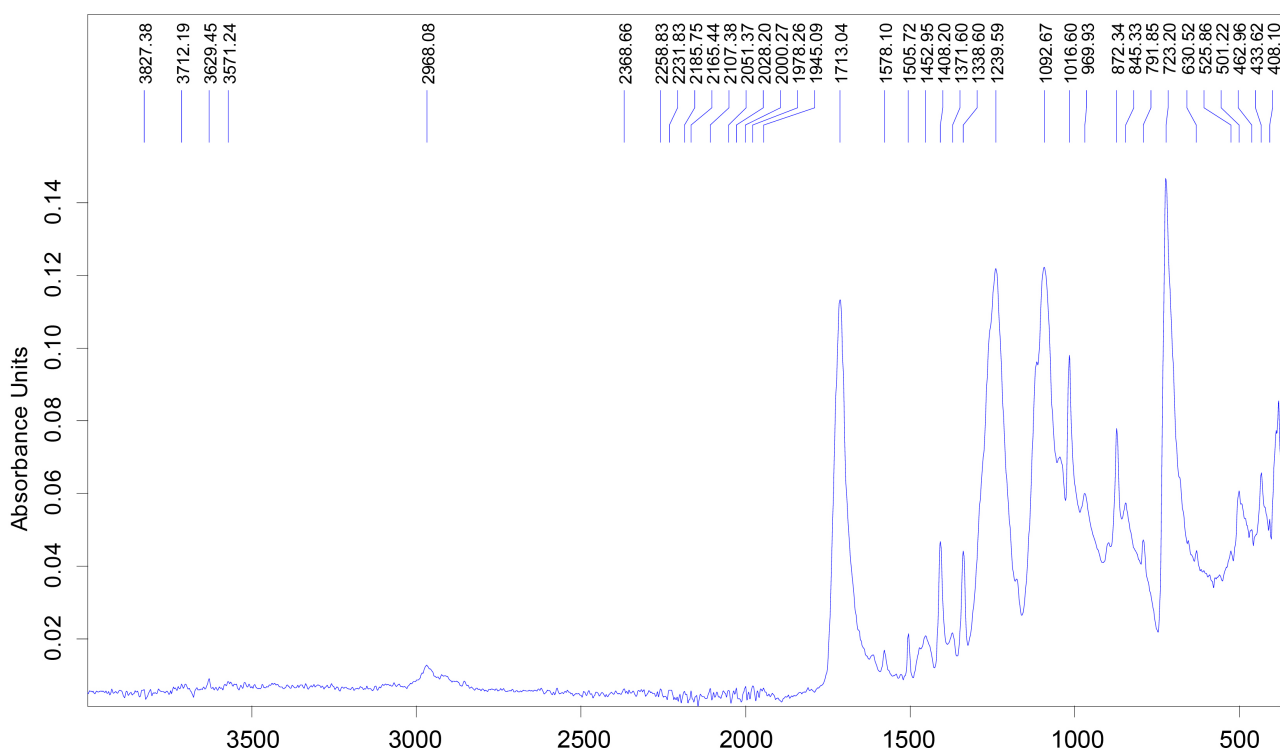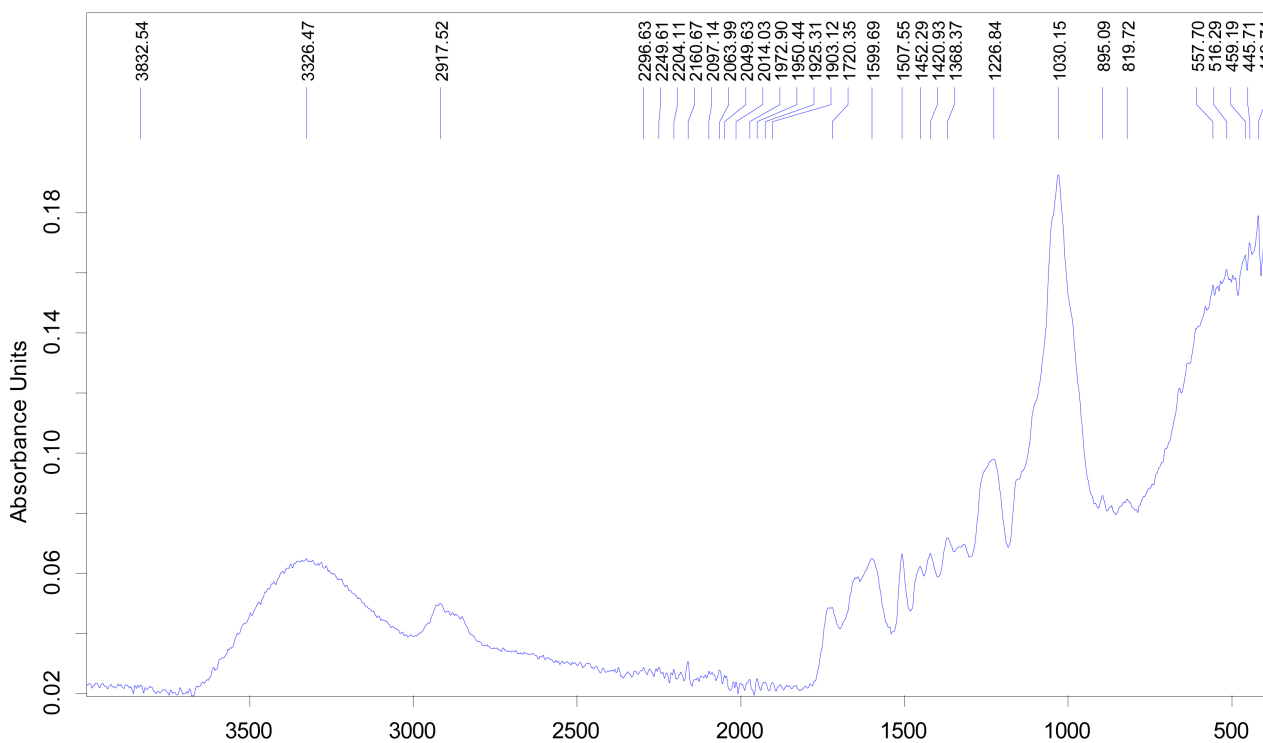

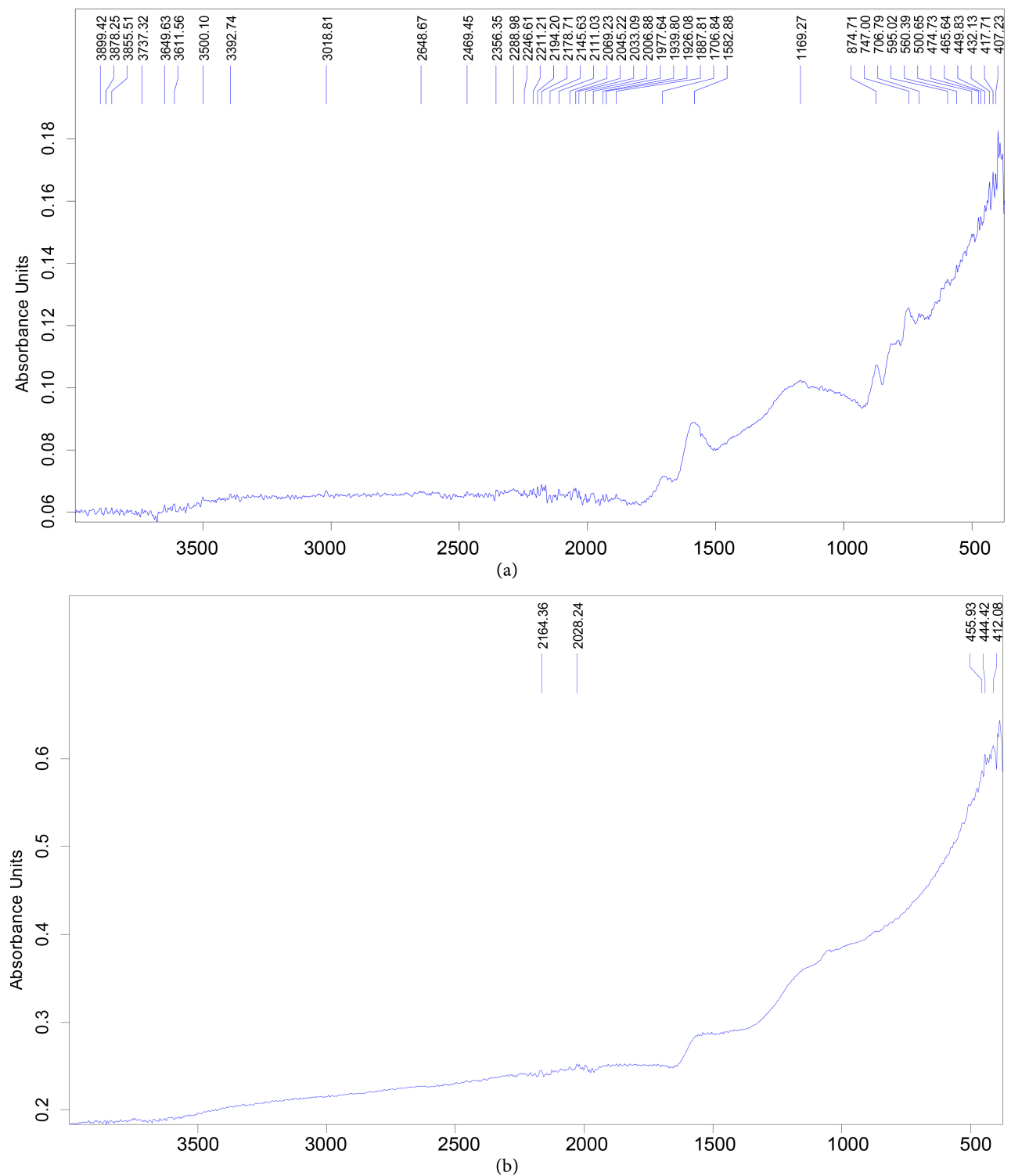
**Figure 4.** FT-IR spectrum of PET.

This region allows to account for substitutions on the benzene rings and to evaluate the degree of condensation of the aromatic rings.

**Figure 5** shows the FT-IR of CS and it reveals that a broad absorption band located between 3600 - 3300 cm$^{-1}$ with a maximum of around 3400 cm$^{-1}$ is characteristic of the O-H elongation vibration of carboxyl, phenols or water absorbed of CS. The band around 2900 cm$^{-1}$ is attributed to the −CH$_3$ asymmetric and symmetric valence vibration. The bands located at 1700 cm$^{-1}$ and 1600 cm$^{-1}$ derived from the C=O elongation vibration in ketone, aldehyde, lactone carbonyl groups and aromatic ring respectively. This indicates the formation of carbonyl-containing groups. The bands from 1470 to 1370 cm$^{-1}$ are a domain that is formed by an overlap of absorption bands attributable to hydroxyl-type moieties on the surfaces and in-plane vibrations of the C-H bond in several C=C-H structures. The bands between 1000 - 500 cm$^{-1}$ are due to the out-of-plane C-H deformation mode in differently substituted aromatic rings. The presence of hydroxyl of phenolic and carboxyl functional groups provides the surface of CS an acidic character while the carbonyl functional groups give a basic character. Therefore, the main surface functional groups present on CS surface have seemed to be carbonyl, ethers and carboxylic acids. These groups are similar to those found on some agricultural lignocellulosic residues [50].

**Figure 6** presents the FT-IR of PETAC and CS/PETAC. The bands around 1700 cm$^{-1}$ and 1600 to 650 cm$^{-1}$ for PETAC (**Figure 6(a)**) and around 1650 cm$^{-1}$ for CS/PETAC (**Figure 6(b)**) are caused by the C=O elongation vibration in ketone, aldehyde, lactone, carbonyl groups and aromatic ring. The bands located



**Figure 5.** FT-IR spectrum of CS.

85

**Figure 6.** FT-IR spectrum of the PETAC (a) and CS/PETAC (b).

from 1070 to 1370 cm$^{-1}$, which are weak bands for CS/PETAC are in a domain that is formed by an overlap of absorption bands attributable to C-O bond and also to the P-O and P=bonds on the surface and in-plane vibrations of the C-H bond in several C=C-H structures. The disappearance of −OH and other func-

tional groups from the precursors to the prepared adsorbents indicates the role played by the activating reagent ($H_3PO_4$) and the PET material.

## 3.4. SEM-EDS Analysis Results

To analyze the surface morphology and elemental composition of the precursors (PET and CS) and the adsorbents synthesized (PETAC and CS/PETAC) their SEM/EDS were performed. **Figure 7** helps to visualize the surface morphology of PET and CS at different resolutions and magnifications.

It can be observed from **Figure 7(a)** that the PET precursor has a random shape with a smooth surface and sharp edges. Moreover, there is a quasi-absence of any hole proving that PET is non-porous. From **Figure 7(b)** it can be seen that the CS surface is rock-like with few pores. Moreover, this surface is very rough



(a)

(b)
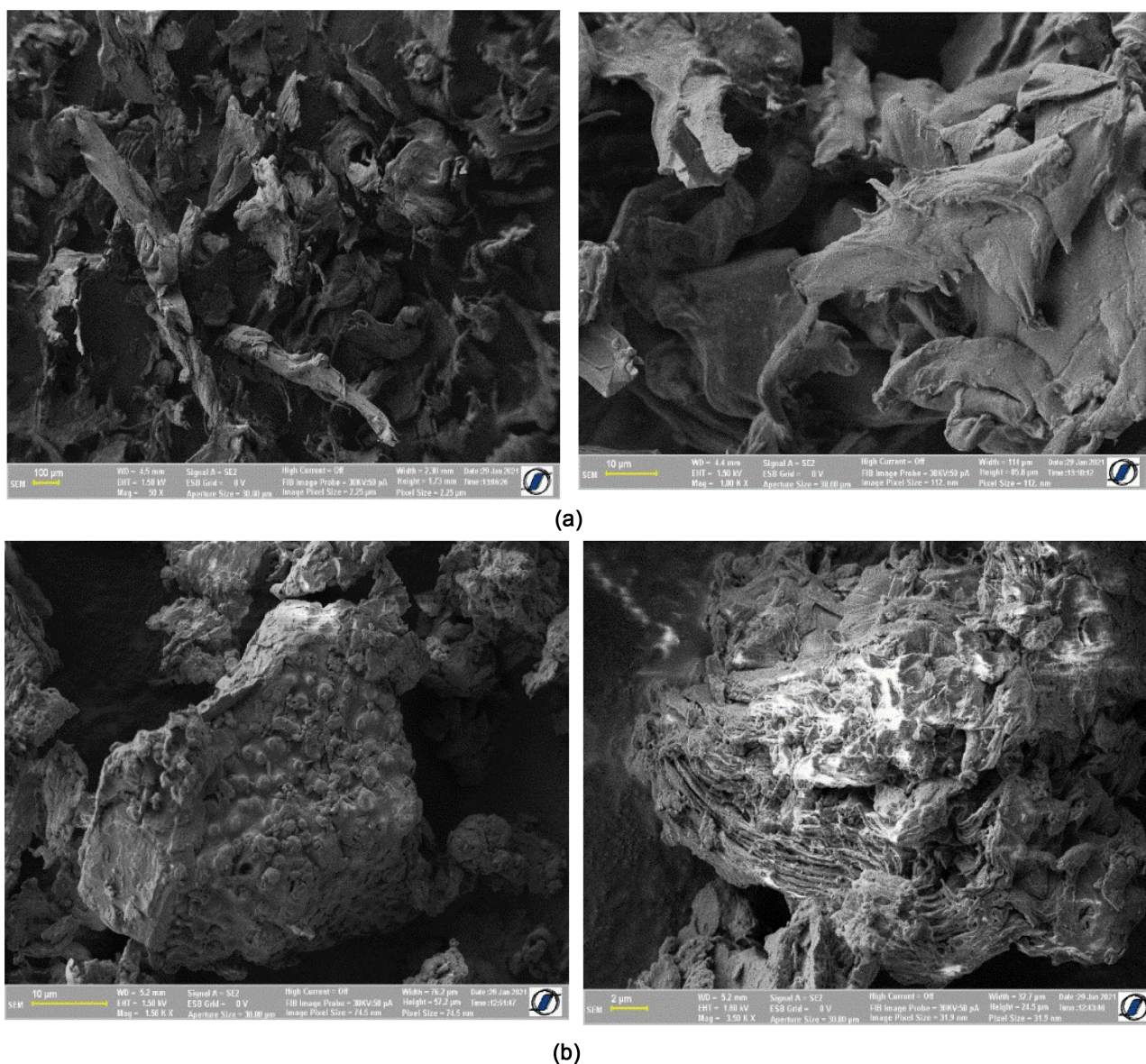
**Figure 7.** SEM images of PET (a) and CS (b).

and shows cracks at high resolutions. The images show a material with a uniformly identical texture with almost no pores, in other words, the pores are less visible. To obtain the elemental composition of some areas of the micrograph given by the SEM, two areas were chosen as shown in Figure 8.

It results from Figure 8(a) show that PET presents only two elements. The most abundant is carbon with an average atomic percentage of 74.61% followed by oxygen with an average atomic percentage of 22.97%. It should be noted that this method of analysis is not sensitive to the hydrogen atom, hence its absence. The difference in the percentage of the elements in the selected zones also shows that the atomic dispersion in the sample is not homogeneous. Its heterogeneity may be due to the initiation and termination of polymer chains during polymerization. From Figure 8(b) it can be seen that the most abundant element is carbon with an average atomic percentage of 63.28% followed by oxygen



**(a)**



**(b)**
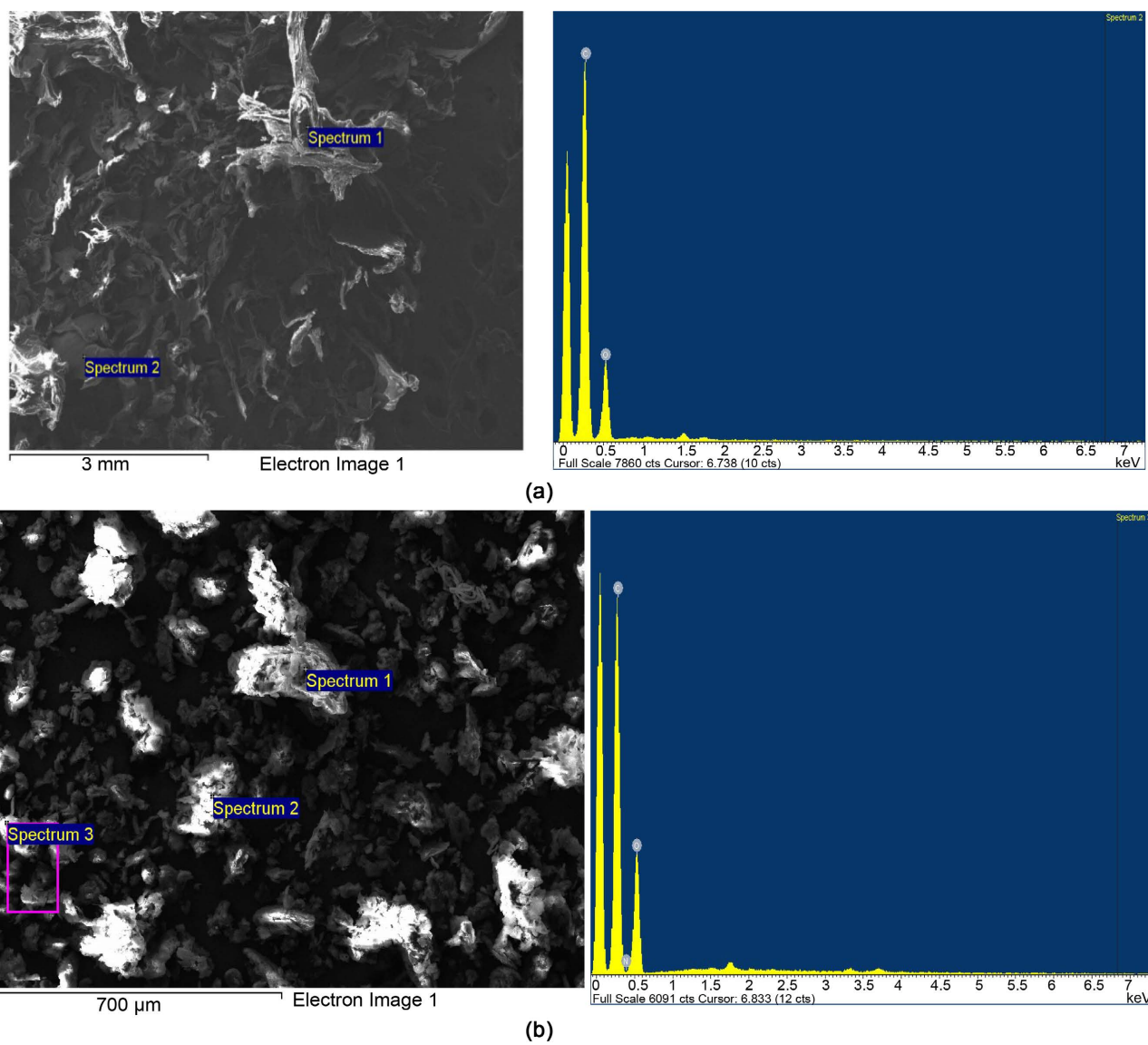
Figure 8. SEM-EDS images of PET (a) and CS (b).

with an average atomic percentage of 29.23% and nitrogen with an average atomic percentage of 7.32%. The difference in the percentage of the elements in the selected areas and the absence of magnesium, silicon and calcium shows that the atomic dispersion in the samples is not homogeneous. Moreover, the white parts observed on CS micrograph give an idea on a certain degree of crystallinity of CS. Figure 9 gives the SEM of PETAC and CS/PETAC at different resolutions and magnifications.

From Figure 9(a), it revealed that PETAC has a rough surface at magnification. It can also be seen that there are many pores on the surface and internal cross-section of PETAC which might result from the spaces between the rough structures on the surface of the prepared material. This porous structure may affect the RhB dye sorption efficiency and is found to have relatively more homogeneous pores with constant diameters. Figure 9(b) shows the micrograph of CS/PETAC which looks aggregate and possess more pore than the



(a)

(b)
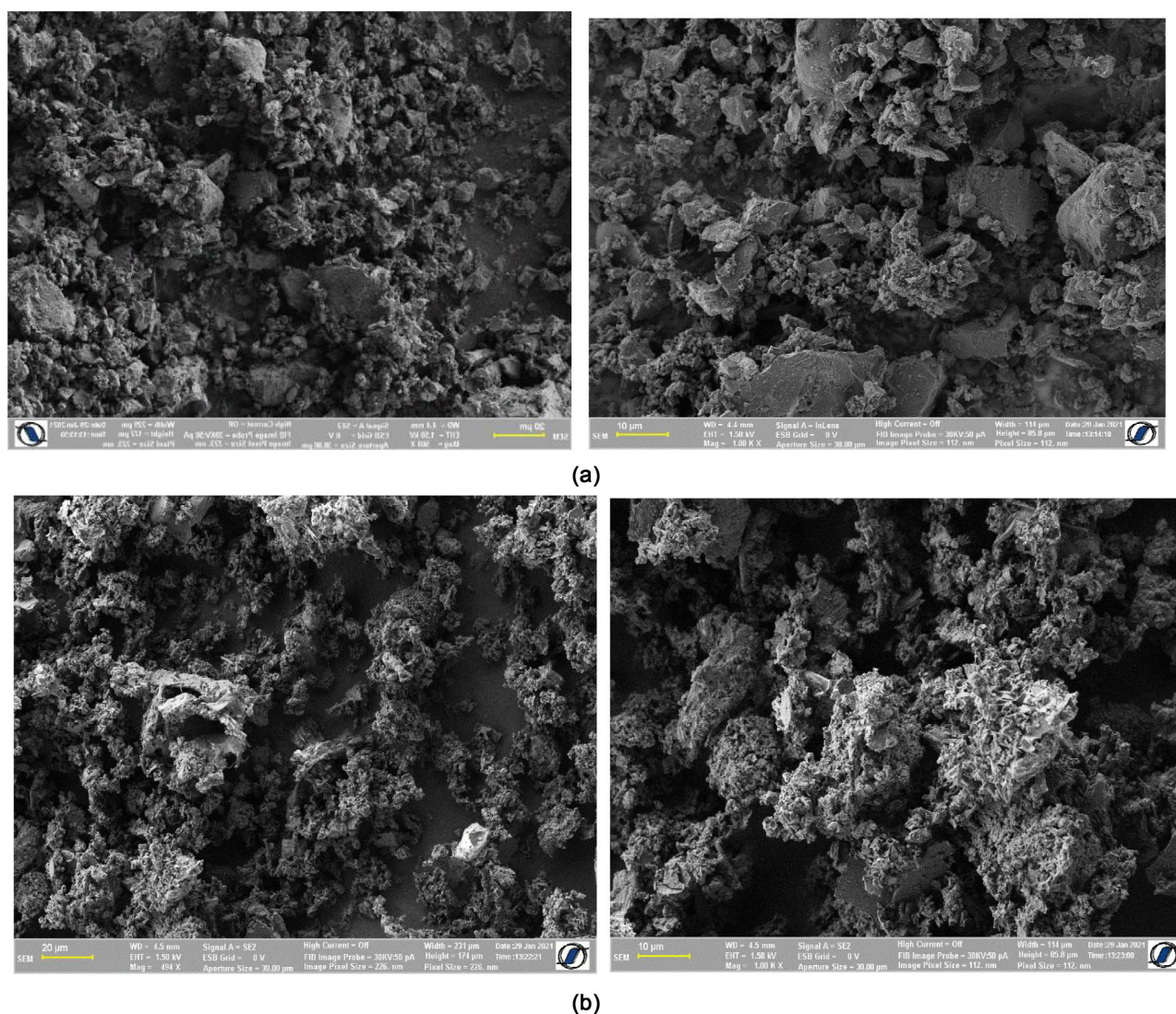
**Figure 9.** SEM images of PETAC (a) and CS/PETAC (b).

activated carbon obtained from PET alone which is in agreement with the results of BHJ calculation from nitrogen adsorption-desorption as seen in Table 1. The resulting micrographs obtained are the consequence of the starting materials used. Moreover, the CS seeds produce many coals with a large pore diameter range in contrast with the PET which produces coals with a uniform pore diameter. Maybe mixing the two PET and CS precursors, allowed the effect of reducing the multiplicity of pores. Therefore, it can be considered a major advantage in the preparation of carbon adsorbents used for adsorption, however for adsorption to take place in the micropores and mesoporous, the adsorbate must pass through the macropores which serve as a highway to the inner structure of carbon adsorbent.

The analysis of the composition of PETAC and CS/PETAC shows that the two adsorbents are constituted mainly by carbon and oxygen atoms with the highest percentage of carbon meanwhile, Figure 10(a) and Figure 10(b) show carbon materials with different textures. This result confirms that CS/PET is a strongly carbonaceous material compared to PETAC. The other atoms like phosphorus and nitrogen either come from the starting materials or the activating reagent. Additionally, the presence of the phosphorus atom may be the result of the reaction of phosphate ions with the precursors.

### 3.5. Textural Properties Analysis Results

The textural properties determination was done by $N_2$ adsorption-desorption using a Micromeritics Surface Analyzer (Quantachrome, NOVA 1000e series, USA). The surface area, pore volumes and pore size distribution were calculated

**Table 1.** Summary of surface characteristics of PETAC and CS/PETAC.

| Parameters | Determination method used | PETAC | CS/PETAC |
|---|---|---|---|
| Specific surface area (mg/g) | BET multipoint | 6.749 | 1282.0 |
| | BJH cumulative desorption surface area | 34.38 | 336.4 |
| | DH cumulative desorption surface area | 34.79 | 340.5 |
| | DFT cumulative surface area | 4.384 | 859.5 |
| Pore volume (cm³/g) | BJH cumulative desorption pore volume | 0.05140 | 0.3941 |
| | DH cumulative desorption pore volume | 0.04998 | 0.3838 |
| | HK micropore volume | 0.002119 | 0.5464 |
| | SF micropore volume | 0.0008673 | 0.3550 |
| | DFT cumulative pore volume | 0.01828 | 0.8248 |
| Pore diameter (nm) | BJH desorption pore diameter | 3.616 | 3.846 |
| | DH desorption pore diameter | 3.616 | 3.846 |
| | HK pore diameter | 0.3675 | 0.3675 |
| | SF pore diameter | 0.4523 | 0.4523 |
| | DFT pore Diameter | 6.225 | 1.543 |
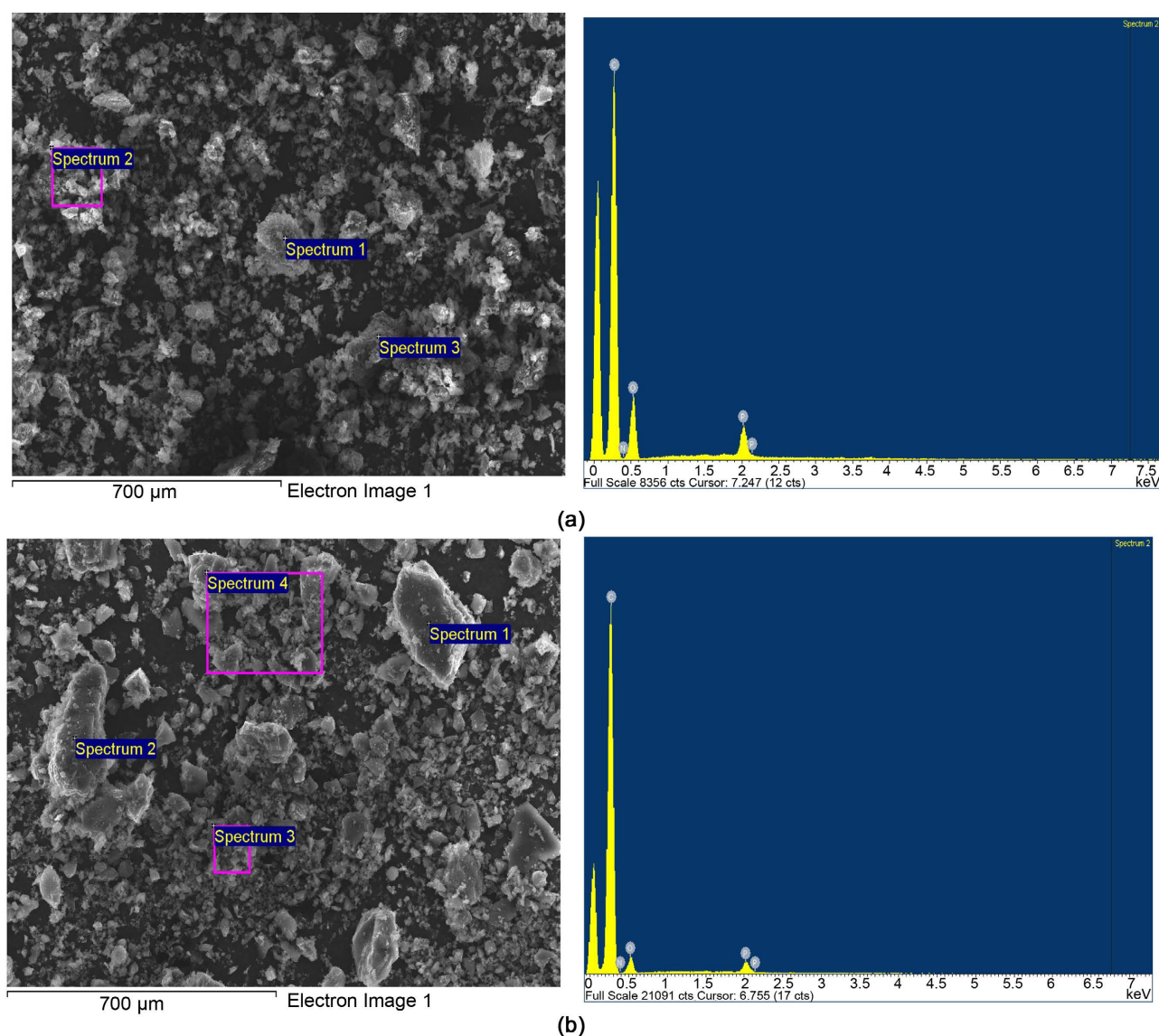
**Figure 10.** SEM-EDS images of PETAC (a) and CS/PETAC (b).

by the Brunauer-Emmett-Teller (BET) multipoint, Dollimore-Heal (DH), Barret-Joyner-Halenda (BJH) and Density Functional Theory (DFT) methods. Table 1 compiles the surface characteristics of PETAC and CS/PETAC according to the different methods used.

According to Table 1, PETAC presented a low multipoint BET surface area (6.749 m²·g⁻¹) compared to CS/PETAC (1282 m²·g⁻¹). Moreover, PETAC has a smaller pore volume from the BJH method (0.05140 cm³/g) while CS/PETAC is greater (0.3941 cm³/g). This significant increase observed in BET surface area and pore volume from PETAC to CS/PETAC may result from the high carbon content in CS/PETAC obtained during the re-enforcement process of the plastic on CS. Moreover, this increase can be attributed to particle arrangement on basic precursors which synergically screened the pores during the composite material preparation. On the other hand, CS/PETAC was found to have a higher

pore diameter compared to PETAC. This can be attributed to the preparation method used which consequently favors the opening of the pores. This large opening of pores could be helpful for the adsorption of large molecules like RhB. The pore diameters for both PETAC and CS/PETAC range between 2 and 50 nm suggesting a dominance of mesoporosity. In addition, the specific surface area of CS/PETAC which is greater than that of PETAC may be considered as a contribution of PET in reinforcing the structural properties of the lignocellulosic material which are the *Canarium schweinfurthii* shells.

# 4. Adsorption Studies Results

## 4.1. Effect of pH

The effect of pH on the RhB adsorbed quantity was investigated under the conditions of 30 min of contact, an adsorbent dose of 0.02 g and an initial concentration of 100 mg/L. According to Figure 11, the increase in pH values was found to have no remarkable effect on RhB adsorbed on both CS/PETAC and PETAC. This little effect of RhB adsorbed onto both cases is between pH 2 to 11. In both cases, there was a slight variation of less than 2% change. This may be due to the fact that an increase in pH values contributes to an increase in hydroxide ions ($OH^-$) in the solution. These hydroxide ions are either neutralized by the positive sites in both cases surface and the electrostatic attractions with cationic dye of RhB which favors adsorption. Meanwhile, there is strong electrostatic repulsion between both cases and cationic RhB which reduces adsorption. A similar situation was observed during photodegrading on $TiO_2$ and ZnO and modified $TiO_2$ nanoparticles [51]-[55]. This observation is consistent with the fact that, in the adsorption process, the pH affects both the RhB degree of ionization and the surface chemistry of the adsorbents. Further, an increase in pH values had no reasonable change in RhB quantity adsorbed because of the protonation and deprotonation of the surface functional groups present on both the adsorbent.
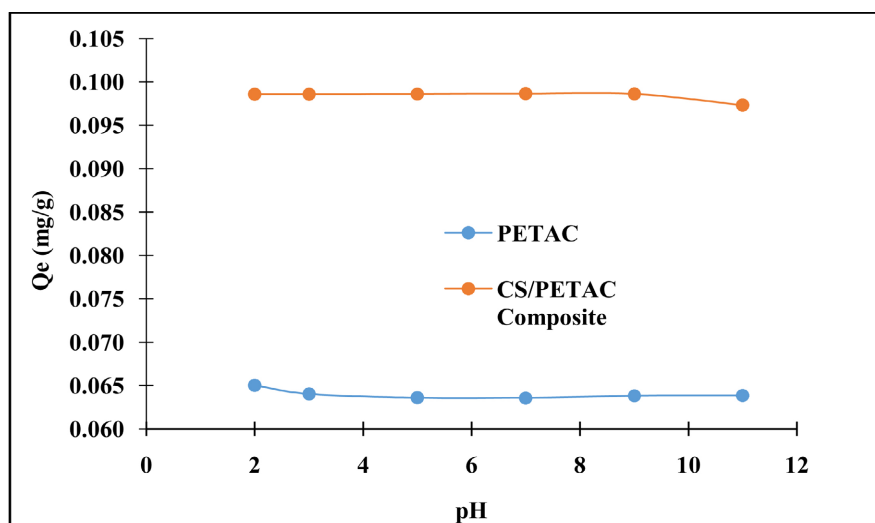


**Figure 11.** Graph of the effect of pH on RhB removal onto PETAC and CS/PETAC.

## 4.2. Effect of Contact Time

The effect of contact time on the RhB removal onto PETAC and CS/PETAC is represented of Figure 12. Since the pH had no effect on PETAC and CS/PETAC adsorbents, the effect of contact time on RhB adsorbed quantity was investigated under the conditions of initial pH of RhB solution, concentration of 100 mg/L and adsorbent dose of 0.02 g a variable time between 0 to 60 min. Figure 12 reveals that the results achieved for the two adsorbents can be seen that the rate of adsorption is faster for PETAC and CS/PETAC within 0 to 5 min of the adsorption process. Then, there is a slowdown leading to an equilibrium state. The rapid increase of the RhB adsorbed quantity during the initial time of adsorption process may be attributed to the availability of large number of adsorption sites. The slowdown and the establishment of equilibrium within 10 min for both PETAC and CS/PETAC is due to the saturation of adsorption sites [26]. The adsorbed quantity at equilibrium were 63.093 mg/g and 98.168 mg/g for PETAC and CS/PETAC respectively. This difference of 35.730% between PETAC and CS/PETAC on the adsorption capacity could be the result of the difference in the physicochemical properties and also the results of synthesis of a composite material with greater adsorption property than PETAC alone. During the production of CS/PETAC composite adsorbent, the aromatization reaction of the composite is reinforced by the presence of the carbon enriched by PET to give the composite a restructured form with higher adsorptive property. Furthermore, the restructuring gives the composite higher surface area (Table 1). The large specific surface area and pore size distribution on composite are favorable for liquid phase adsorption of organic pollutants such as dyes in terms of adsorption efficiency. The difference in adsorption capacity which is considered insignificant can be explained by the fact, the Rhodamine B adsorption does not only depend on the large specific surface area of 1282 $m^2 \cdot g^{-1}$ obtained but also on the surface functional groups present on both adsorbents.
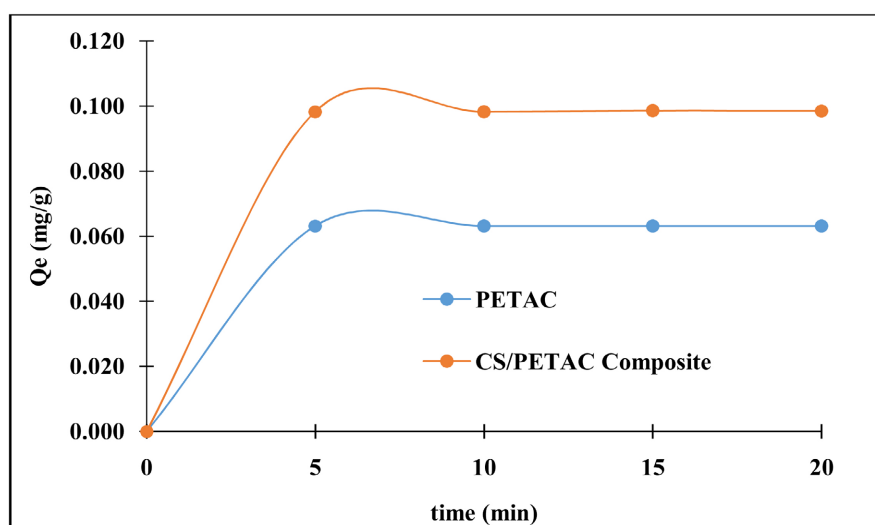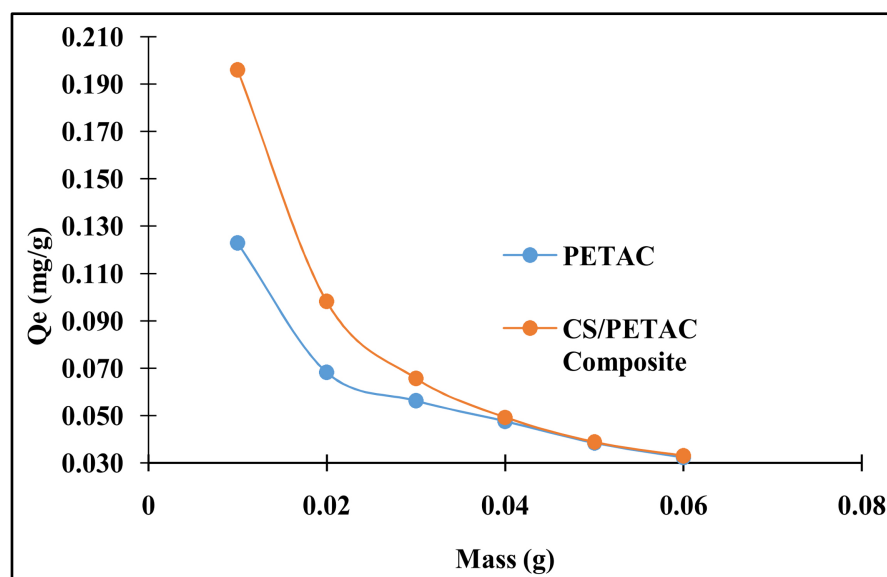


**Figure 12.** Graph of the effect of contact time on RhB removal onto PETAC and CS/PETAC.

## 4.3. Effect of Adsorbent Dose

The effect of the adsorbent dose on the RhB adsorption on PETAC and CS/PETAC was investigated at initial pH of MB solution with initial concentration of 100 mg/L and adsorbent dose varied from 0.01 to 0.06 g and for contact time of 35 and 10 min for PETAC and CS/PETAC respectively. **Figure 13** shows the RhB adsorbed quantity versus the mass of synthesized adsorbents under the optimum conditions. It is seen that, RhB adsorption decreases with an increase in adsorbent dose for both adsorbent. Similar results were observed by Bhat *et al.*, 2017. The rate of the decrease is more prominent at higher amounts of adsorbate concentration. Significant RhB adsorption is achieved for PETAC and CS/PETAC adsorbent dose of 0.02 g. This observation may be due to the fact that, at lower adsorbent dose, the adsorption sites are available while at higher adsorbent dose, there is an agglomeration of adsorbent particles leading to particle size aggregation reducing the available specific surface area and the increased in the diffusional path length [19].

## 4.4. Effect of Initial Concentration

The variation of the RhB initial concentration was carried out in the range of 50 to 100 mg/L at an initial pH of RhB solution of 2 with an adsorbent dose of 0.02 g and for a contact time of 10 min for PETAC and CS/PETAC respectively. **Figure 14** exhibits the RhB adsorbed quantity for the two adsorbents. The results showed that, as the initial concentration of RhB increases, the adsorbed quantity per unit of adsorbent mass also increases. The adsorbed quantity increases from 48.528 to 98.213 mg/g for CS/PETAC, while it increases from 40.169 to 75.575 mg/g for PETAC. The increase of adsorbed quantity is mainly due to the increase of effective collisions in solution between the RhB dye on the respective



**Figure 13.** Graph of the effect of adsorbent dose on RhB removal onto PETAC and CS/PETAC.
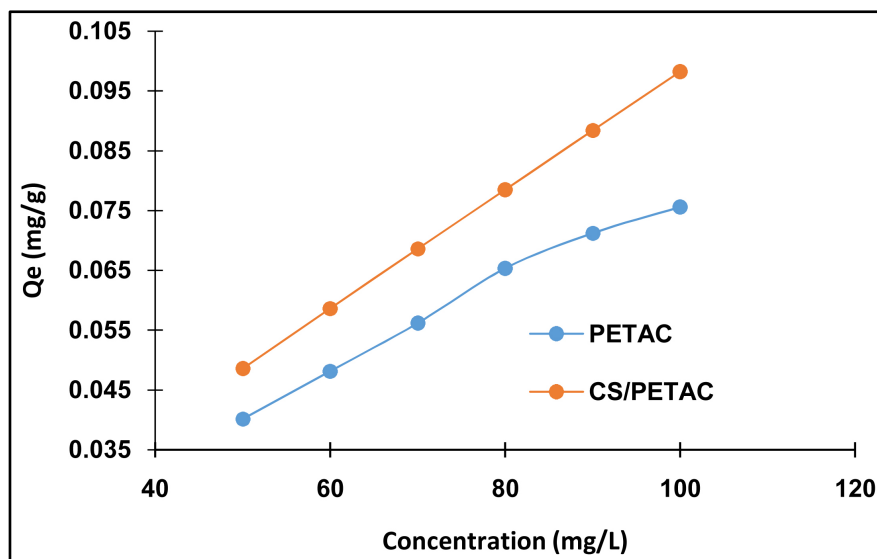
**Figure 14.** Graph of the effect of initial concentration on RhB removal onto PETAC and CS/PETAC.

adsorbents. This ineffective collision decreases the activation energy of the colliding particles hence the decrease in force helps to overcome the mass transfer resistance between the aqueous and solid phases [19] [26]. This decrease in activation energy favors effective collision which favors adsorption of RhB adsorption onto the respective adsorbents. The maximum adsorption quantity of Rhodamine B on PETAC and CS/PETAC are compared in Table 2.

# 5. Non-Linear Adsorption Isotherms and Kinetic Modeling

## 5.1. Isotherm Studies

The plots of the four RhB adsorption isotherms onto PETAC and CS/PETAC are presented in Figure 15 and their calculated values parameters are reported in Table 3. From Table 3, Langmuir and Tempkin isotherm could not explain the RhB dye adsorption phenomenon onto PETAC because of their respective negative correlation coefficient ($R^2$) values. Freundlich isotherm was the most appropriate to describe the RhB dye adsorption data suggesting a multilayer adsorption process onto PETAC and CS/PETAC with their respective $R^2$ values close to unity. For both two adsorbents, the high $R^2$ values of the Freundlich model were accredited by the goodness of fit of the non-linear isotherm functions. This could be attributed to the coulombian interaction between adsorbent surface functional groups with those of RhB dye. This result confirms why the Freundlich model is the best to explain the adsorption process. Additionally, the physical process is suitable for multilayer adsorption, unlike the Langmuir model which favors monolayer adsorption.

## 5.2. Kinetics Studies

The kinetic curves are shown in Figure 16 while their kinetic parameters are

**Table 2.** Comparative results of the adsorption of Rhodamine B onPETAC, and CS/PETA) with other adsorbents.

| Materials | Quantity adsorbed at equilibrium | References |
|---|---|---|
| Gelatin/activated carbon composite beads (GE/AC) | 256.41 mg/g | [56] |
| Zinc chloride/ferric chloride activation | 371 mg/g | [57] |
| Coconut Shell Activated Carbon/$CoFe_2O_4$ Composite (CAC) | 94.08 mg/g | [58] |
| WO3/Activated carbon composite (WO3/AC) | 797.9 mg/g | [59] |
| Polyethylene Terephthalate Activated Carbon (PETAC) | 75.575 mg/g | Present work |
| *Canarium schweinfurthii*/Polyethylene Terephthalate Activated Carbon (CS/PETAC) | 98.213 mg/g | Present work |

**Table 3.** Summary of relative non-linear isotherm constants and their respective determination coefficients ($R^2$, *RMSE* and $\chi^2$) for the RhB adsorption onto PETAC and CS/PETAC composite.

| Models | Parameters | Adsorbent | |
|---|---|---|---|
| | | PETAC | CS/PETAC |
| Langmuir | $Q_m$ mg/g | 21.248 | 1548.154 |
| | $K_L$ | 0.176 | 0.031 |
| | $R_L$ | 0.102 | 0.394 |
| | $R^2$ | −0.130 | 0.721 |
| | *RMSE* | 7.254 | 10.868 |
| | $\chi^2$ | 9.545 | 27.479 |
| Freundlich | $K_F$ | 1.249 | 1.000 |
| | $1/n$ | 0.926 | 1.000 |
| | $R^2$ | 0.996 | 1.000 |
| | *RMSE* | 0.355 | 0.002 |
| | $\chi^2$ | 0.050 | $2.502 \times 10^{-7}$ |
| Tempkin | $K_T$ | 15361965.820 | 2.576 |
| | $b$ | 2574.230 | 47.134 |
| | $R^2$ | −0.056 | 0.656 |
| | *RMSE* | 7.013 | 12.056 |
| | $\chi^2$ | 9.867 | 7.647 |
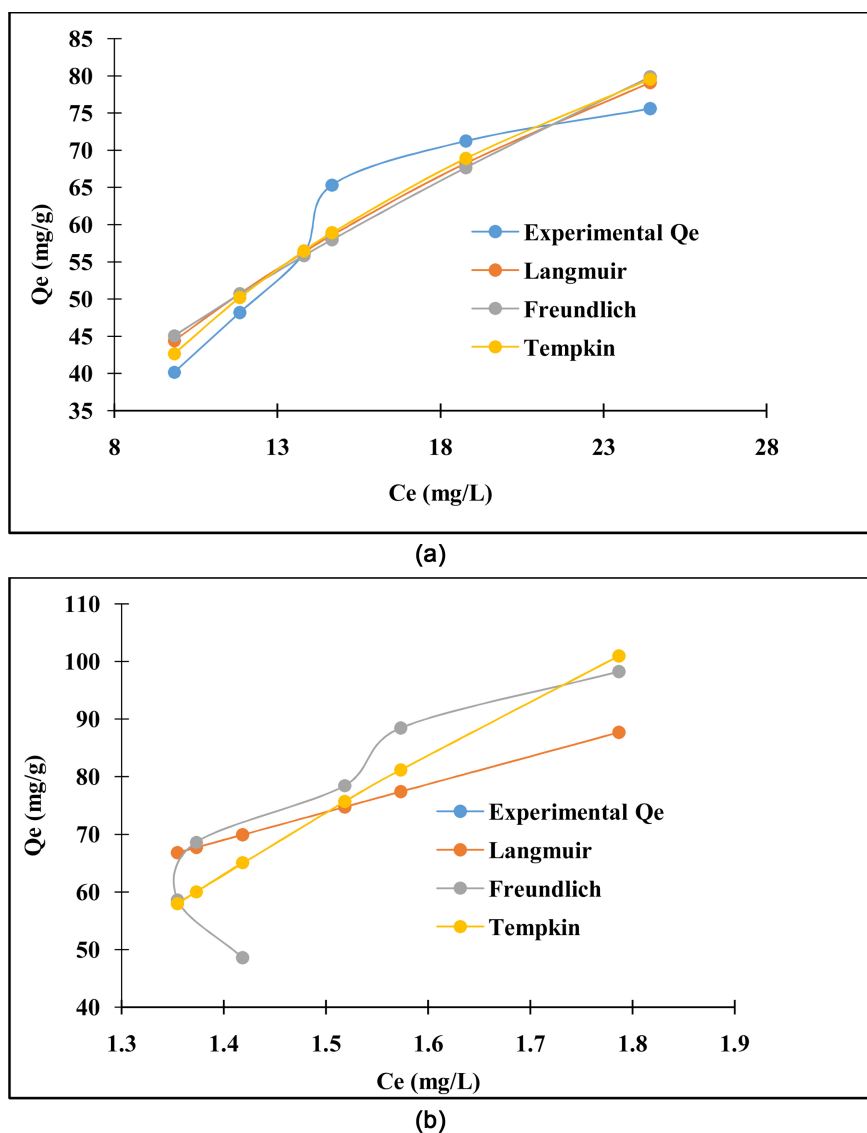
**Figure 15.** Representation of the isotherm models plot for PETAC (a) and CS/PETAC (b).

gathered in Table 4.

From Table 4, the pseudo-first and pseudo-second-order kinetic models both elucidate the RhB adsorption mechanism onto PETAC and CS/PETAC based on their high correlation coefficient of unity and their experimental and theoretical quantity adsorbed which are closer. This suggests that both chemisorption and physisorption phenomena have a significant dominant effect on the RhB dye adsorption process. This effect was also substantiated for their *RMSE* and $\chi^2$ values which were 0.015 and 0.002 for PETAC and 0.137 and 0.002 for CS/PETAC respectively which of course are low, especially in the case of the pseudo first-order kinetic model. In the case of the pseudo-second-order kinetic model, the high correlation coefficient and low *RMSE* and $\chi^2$ values were 0.015 and 3.732 for PETAC and 0.091 and 0.001 for CS/PETAC respectively. This low value also implies that the chemisorption phenomenon seems to be important.
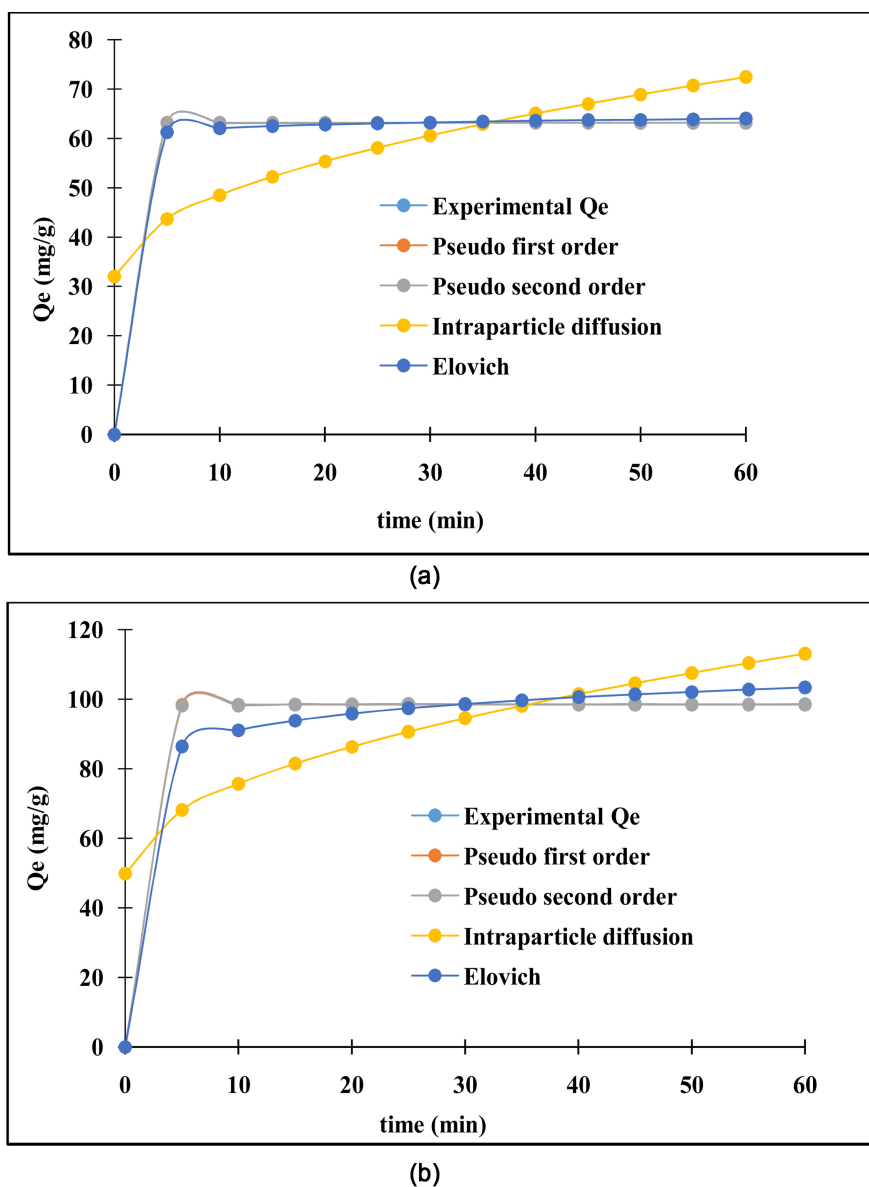
**Figure 16.** Representation of the kinetic models plot for PETAC (a) and CS/PETAC (b).

Furthermore, for both the two adsorbents, the Elovich model suggests by the initial adsorption speed constant rate ($\alpha$) which is greater compared to the desorption coefficient ($\beta$) in PETAC and CS/PETAC, it certifies that the RhB dye adsorption process is governed by the chemisorption phenomenon. This model was also substantiated by the relatively small *RMSE* and $\chi^2$ values. In addition, the RhB dye adsorption mechanism in both cases could not be clearly elucidated by the pore intra-particle pore diffusion model because of its low correlation constant. However, in both cases, the thickness of the resistance barrier force (C) being greater than unity clarifies the notion that the pore intra-particle diffusion is not the rate-limiting step and reinforces the postulate that intra-particle diffusion was not the only controlling step for RhB dye adsorption and the process is also controlled by boundary layer diffusion [47].

**Table 4.** Summary of the different relative non-linear kinetic constants and their respective determination coefficients ($R^2$, *RMSE* and $\chi^2$) for the adsorption of RhB dye onto PETAC and CS/PETAC composite.

| Models | Parameters | Adsorbent | |
|---|---|---|---|
| | | PETAC | CS/PETAC |
| Pseudo-first-order | $Q_e\,(exp)$ | 63.093 | 98.168 |
| | $Q_e\,(cal)$ | 63.116 | 98.454 |
| | $K_1$ | 4.986 | 3.000 |
| | $R^2$ | 1.000 | 1.000 |
| | *RMSE* | 0.015 | 0.137 |
| | $\chi^2$ | 0.002 | 0.002 |
| Pseudo-second-order | $Qe\,(cal)$ | 63.116 | 98.857 |
| | $K_2$ | 2329.737 | 0.500 |
| | $R^2$ | 1.000 | 1.000 |
| | *RMSE* | 0.015 | 0.091 |
| | $\chi^2$ | 3.732 | 0.001 |
| Elovich | $\alpha$ | $6..152 \times 10^{23}$ | 425506.593 |
| | $\beta$ | 0.919 | 0.146 |
| | $R^2$ | 0.998 | 0.968 |
| | *RMSE* | 0.819 | 5.123 |
| | $\chi^2$ | 0.119 | 3.160 |
| Intraparticule diffusion | $K_{id}$ | 5.211 | 8.152 |
| | $C$ | 32.045 | 49.867 |
| | $R^2$ | 0.809 | 0.209 |
| | *RMSE* | 13.558 | 21.098 |
| | $\chi^2$ | 19.668 | 80.374 |

## 6. Conclusion

The preparation of two carbon materials (PETAC and CS/PETAC) has been successfully achieved and the paper highlighted the key role of PET in the formulation of a composite material and the application of both the two materials on RhB dye removal in aqueous solution. The adsorption results obtained are consistent with the fact that adsorption does not only depends on the large specific surface area but also on the surface functional groups present on the materials. The FT-IR spectra of CS/PETAC show a drastic modification in the different surface functional groups and was confirmed by the SEM-EDS analysis showing a high percentage of carbon in CS/PETAC. The $N_2$ adsorption-desorption isotherm according to BET method shows the higher specific surface area, pore volume and pore diameter for CS/PETAC compared to PETAC. This result demonstrated the synergic addition effect of the PET during the structuration of

the composite material. The strength of the pore capacity and surface functional group of the prepared samples were unmasked on the retention of RhB dye from aqueous solution. CS/PETAC did not only shows high value of specific surface area but also demonstrated higher adsorption capacity than PETAC. The amount of RhB dye uptake varied from 48.528 to 98.213 mg/g for CS/PETAC, while it increased from 40.169 to 75.575 mg/g for PETAC. Additionally, the quantity of RhB retained decreases as the initial dye concentration increases for PETAC while that of CS/PETAC increases as the RhB dye initial concentration increases. This was attributed to the consequence of restructuration of CS carbon matrix against PET during the carbonization and activation process. The restructuration and the increase in carbon content brought by PET material have enhanced the composite adsorption process. The isotherm and kinetic modeling of the experimental data using non-linear regression shows that, Freundlich isotherm model, pseudo-first and pseudo-second order kinetic model gave the best fit to explain the adsorption equilibrium and mechanism on both the two adsorbents. It was also found that the RhB dye adsorption mechanism was dominant chemisorption with higher adsorption speed constant ($\alpha$) of the Elovich kinetic model.

## Acknowledgements

## Declaration of Interest

The authors declare no conflict of interest.

## References

[1] Sharma, M., Dubey, A. and Pareek, A. (2014) Algal Flora on Degrading Polythene Waste. *CIBTech Journal of Microbiology*, **3**, 43-47.

[2] Mehdi, S., Djamel, B., Abdelouahed, K. and Mohamed, I.H. (2017) The Possibility of Making a Composite Material from Waste Plastic. *Energy Procedia*, **119**, 163-169. https://doi.org/10.1016/j.egypro.2017.07.065

[3] Kumari, B. and Srivastava, V. (2016) Effect of Waste Plastic and Fly Ash on Mechanical Properties of Rigid Pavement. *International Journal of Civil Engineering*, **7**, 247-256.

[4] Khanday, W.A., Marrakchi, F., Asif, M. and Hameed, B.H. (2016) Mesoporous Zeolite-Activated Carbon Composite from Oil Palm Ash as an Effective Adsorbent for Methylene Blue. *Journal of the Taiwan Institute of Chemical Engineers*, **70**, 32-41.

[5] Swapnil, K.K., Amit, G.D., Mahendra, S.D. and Vikram, B.P. (2015) Microbial Degradation of Plastic: A Review. *Journal of Biochemical Technology*, **6**, 952-961.

[6] Raziyafathima, M., Praseetha, P.K. and Rimal, I.R.S. (2016) Microbial Degradation

of Plastic Waste: A Review. *Journal of Pharmaceutical, Chemical and Biological Sciences*, **4**, 231-242.

[7]     Margaret, P.T., Ravindra, V.S., Phanikumar, B.S., Chandar, C.V. and Chowdary, K.A. (2020) Properties of Concrete by Partial Replacement of Cement with Activated Charcoal and Fine Aggregate with Plastic Powder. *Zeichen Journal*, **6**, 97-112.

[8]     Rajmohan, K.S., Ramya, C. and Sunita, V. (2019) Plastic Pollutants: Waste Management for Pollution Control and Abatement. *Current Opinion in Environmental Science & Health*, **12**, 72-84.
https://doi.org/10.1016/j.coesh.2019.08.006

[9]     Dumbili, E. and Henderson, L. (2020) The Challenge of Plastic Pollution in Nigeria. In: Letcher, T.M., Ed., *Plastic Waste and Recycling*, Elsevier, Amsterdam, 569-583.
https://doi.org/10.1016/B978-0-12-817880-5.00022-0

[10]    Wang, R., Meng, T.T., Zhang, B.W., Chen, C.C. and Li, D.G. (2021) Preparation and Characterization of Activated Carbon/Ultra-High Molecular Weight Polyethylene Composites. *Polymer Composites*, **42**, 2728-2736.

[11]    Shahnawaz, M., Sangale, M.K. and Ade, A.B. (2019) Bioremediation Technology for Plastic Waste. Springer, Berlin, 1-139.

[12]    Woo, I.J., Jin, W.L., Young, M.B. and Ok, P.O. (2016) Development of a PP/Carbon/CNT Composite Electrode for the Zinc/Bromine Redox Flow Battery. *Macromolecular Research*, **24**, 276-281. https://doi.org/10.1007/s13233-016-4037-1

[13]    Yang, J.B., Yu, S.Y., Chen, W.T. and Chen, Y.B. (2019) Rhodamine B Removal from Aqueous Solution by CT269DR Resin: Static and Dynamic Study. *Adsorption Science & Technology*, **37**, 709-728. https://doi.org/10.1177/0263617419887238

[14]    Le, P.H., Huu, T.V., Thi, T.H.N., Van, Q.N. and Phan, Q.T. (2020) Coconut Shell Activated Carbon/CoFe$_2$O$_4$ Composite for the Removal of Rhodamine B from Aqueous Solution. *Journal of Chemistry*, **2020**, Article ID: 9187960.
https://doi.org/10.1155/2020/9187960

[15]    Zahir, A., Aslam, Z., et al. (2017) Development of Novel Cross-Linked Chitosan for the Removal of Anionic Congo Red Dye. *Journal of Molecular Liquids*, **244**, 211-218.

[16]    Kumar, V., Singh, M., Behera, K. and Pandey, S. (2020) Ionic Liquid Induced Removal of Rhodamine B from Water. *Journal of Molecular Liquids*, **319**, Article ID: 114195. https://doi.org/10.1016/j.molliq.2020.114195

[17]    Rehman, U.Z.U., Aslam, Z., Shawabkeh, R.A., Hussein, I.A. and Mahmood, N. (2020) Concurrent Adsorption of Cationic and Anionic Dyes from Environmental Water on Amine Functionalized Carbon. *Water Science & Technology*, **81**, 466-478.

[18]    Wang, M., Xie, R., Chen, Y., Pu, X., Jiang, W. and Yao, L. (2018) A Novel Mesoporous Zeolite-Activated Carbon Composite as an Effective Adsorbent for Removal of Ammonia-Nitrogen and Methylene Blue from Aqueous Solution. *Bioresource Technology*, **268**, 726-732.
https://doi.org/10.1016/j.biortech.2018.08.037

[19]    Nasrullah, A., Bhat, A.H., Naeem, A., Isa, M.H. and Danish, M. (2017) High Surface Area Mesoporous Activated Carbon-Alginate Beads for Efficient Removal of Methylene Blue. *International Journal of Biological Macromolecules*, **107**, 1792-1799.

[20]    Akhtar, A., Aslam, Z., Asghar, A., Bello, M.M. and Raman, A.A.A. (2020) Electrocoagulation of Congo Red Dye-Containing Wastewater: Optimization of Operational Parameters and Process Mechanism. *Journal of Environmental Chemical Engineering*, **8**, Article ID: 104055.

https://doi.org/10.1016/j.jece.2020.104055

[21] Abbasi, S. (2018) Investigation of the Enhancement and Optimization of the Photocatalytic Activity of Modified $TiO_2$ Nanoparticles with $SnO_2$ Nanoparticles Using Statistical Method. *Materials Research Express*, **5**, Article ID: 066302. https://doi.org/10.1088/2053-1591/aac7f4

[22] Abbasi, S., Hasanpour, M., Ahmadpoor, F., Sillanpää, M., Dastan, D. and Achour, A. (2019) Application of the Statistical Analysis Methodology for Photodegradation of Methyl Orange Using a New Nanocomposite Containing Modified $TiO_2$ Semiconductor with $SnO_2$. *International Journal of Environmental Analytical Chemistry*, **101**, 208-224. https://doi.org/10.1080/03067319.2019.1662414

[23] Abbasi, S., Ahmadpoor, F., Imani, M. and Ekrami-Kakhki, M.-S. (2019) Synthesis of Magnetic $Fe_3O_4$@ZnO@Graphene Oxide Nanocomposite for Photodegradation of Organic Dye Pollutant. *International Journal of Environmental Analytical Chemistry*, **100**, 225-240. https://doi.org/10.1080/03067319.2019.1636038

[24] Abbasi, S. (2019) Adsorption of Dye Organic Pollutant Using Magnetic ZnO Embedded on the Surface of Graphene Oxide. *Journal of Inorganic and Organometallic Polymers and Materials*, **30**, 1924-1934.

[25] Kouotou, D., Mohammed, G., Ndi, J.N., Luisa, M.P.M., Meriam El, O., Ketcha, J.M. and El Khadir, G. (2021) Removal of Metallic Trace Elements ($Pb^{2+}$, $Cd^{2+}$, $Cu^{2+}$ and $Ni^{2+}$) from Aqueous Solution by Adsorption onto Cerium Oxide Modified Activated Carbon. *Environmental Monitoring and Assessment*, **193**, Article No. 467. https://doi.org/10.1007/s10661-021-09267-9

[26] Odogu, A.N., *et al.* (2020) Effect of Doping Activated Carbon Based *Ricinodendron heudelotii* Shells with AgNPs on the Adsorption of Indigo Carmine and Its Antibacterial Properties. *Arabian Journal of Chemistry*, **13**, 5241-5253. https://doi.org/10.1016/j.arabjc.2020.03.002

[27] Saini, J., Garg, V.K., Gupta, R.K. and Kataria, N. (2017) Removal of Orange G and Rhodamine B Dyes from Aqueous System Using Hydrothermally Synthesized Zinc Oxide Loaded Activated Carbon (ZnO-AC). *Journal of Environmental Chemical Engineering*, **5**, 884-892.

[28] Ding, L.L., Zou, B., Gao, W., *et al.* (2014) Adsorption of Rhodamine-B from Aqueous Solution Using Treated Rice Husk-Based Activated Carbon. *Colloids and Surfaces A*: *Physicochemical and Engineering Aspects*, **446**, 1-7. https://doi.org/10.1016/j.colsurfa.2014.01.030

[29] Somsesta, N., Sricharoenchaikul, V. and Aht-Ong, D. (2020) Adsorption Removal of Methylene Blue onto Activated Carbon/Cellulose Biocomposite Films: Equilibrium and Kinetic Studies. *Materials Chemistry and Physics*, **240**, Article ID: 122221. https://doi.org/10.1016/j.matchemphys.2019.122221

[30] Kouotou, D., Ghalit, M., El Ouahabi, M. and Gharibi, E.K. (2021) Removal of Formaldehyde and Methylene Blue from Aqueous Solution by Adsorption on Cerium-Doped Activated Carbon: A Comparative Study. *International Journal of Environmental Analytical Chemistry*, **103**, 8542-8560. https://doi.org/10.1080/03067319.2021.1991335

[31] Tahira, I., Aslam, Z., Abbas, A., Monimul-Mehboob, M., Ali, S. and Asghar, A. (2019) Adsorptive Removal of Acidic Dye onto Grafted Chitosan: A Plausible Grafting and Adsorption Mechanism. *International Journal of Biological Macromolecules*, **1**, 1209-1218.

[32] Ai, L.H., Li, M. and Li, L. (2011) Adsorption of Methylene Blue from Aqueous Solution with Activated Carbon/Cobalt Ferrite/Alginate Composite Beads: Kinetics,

Isotherms, and Thermodynamics. *Journal of Chemical & Engineering Data*, **56**, 3475-3483. https://doi.org/10.1021/je200536h

[33] Marrakchi, F., Bouaziz, M. and Hameed, B.H. (2017) Activated Carbon-Clay Composite as an Effective Adsorbent from the Spent Bleaching Sorbent of Olive Pomace Oil: Process Optimization and Adsorption of Acid Blue 29 and Methylene Blue. *Chemical Engineering Research and Design*, **128**, 221-230. https://doi.org/10.1016/j.cherd.2017.10.015

[34] Ahmad, A., Jini, D., Aravind, M., Parvathiraja, C., Ali, R., Zaheer, K.M. and Ahmad, A. (2020) A Novel Study on Synthesis of Egg Shell Based Activated Carbon for Degradation of Methylene Blue via Photocatalysis. *Arabian Journal of Chemistry*, **13**, 8717-8722.

[35] Aslam, Z., Anait, U., Abbas, A., Ihsanullah, I., Irshad, U. and Mahmood, N. (2020) Adsorption of Carbon Dioxide onto Activated Carbon Preparedfrom Lawn Grass. *Biomass Conversion and Biorefinery*, 1-11.

[36] Mazaheri, H., Ghaedi, M., Asfaram, A. and Hajati, S. (2016) Performance of CuS Nanoparticle Loaded on Activated Carbon in the Adsorption of Methylene Blue and Bromophenol Blue Dyes in Binary Aqueous Solutions: Using Ultrasound Power and Optimization by Central Composite Design. *Journal of Molecular Liquids*, **219**, 667-676. https://doi.org/10.1016/j.molliq.2016.03.050

[37] Benhouria, A., Islam, M.A., Zaghouane-Boudiaf, H., Boutahala, M. and Hameed, B.H. (2015) Calcium Alginate-Bentonite-Activated Carbon Composite Beads as Highly Effective Adsorbent for Methylene Blue. *Chemical Engineering Journal*, **270**, 621-630. https://doi.org/10.1016/j.cej.2015.02.030

[38] Sattar, M., Hayeeye, F., Chinpa, W. and Sirichote, O. (2017) Preparation and Characterization of Poly(lactic acid)/Activated Carbon Composite Bead via Phase Inversion Method and Its Use as Adsorbent for Rhodamine B in Aqueous Solution. *Journal of Environmental Chemical Engineering*, **5**, 3780-3791.

[39] Kulikova, Yu.V., Farberova, E.A., Slyusar, N.N. Il'inykh, G.V. and Korotaev, V.N. (2019) Feasibility Assessment for Production of Sorbents Based on Secondary Carbon Fibers. *Fibre Chemistry*, **51**, 34-40. https://doi.org/10.1007/s10692-019-10056-x

[40] Maguie, K.A., Nsami, N.J., Daouda, K., *et al*. (2017) Adsorption Study of the Removal of Copper(II) Ions Using Activated Carbon Based *Canarium schweinfurthii* Shells Impregnated with ZnCl$_2$. *IRA International Journal of Applied Sciences*, **8**, 18-30. https://doi.org/10.21013/jas.v8.n1.p2

[41] Maguie, K.A., Nsami, N.J., Daouda, K., *et al*. (2017) Activated Carbon Based *Canarium scheweinfurthii* Shells for the Removal of Nitrate Ions from Aqueous Solution. *International Journal on Engineering, Science and Technology*, **6**, 805-815.

[42] Rahman, A.N., *et al*. (2017) Removal of Micro Pollutants from Aqueous Solution Using Activated Carbons from PET Waste. *Canadian Journal of Applied Sciences*, **11**, 4131-4140.

[43] Christian, N.S., Anagho, G.S. and Ngomo, H.M. (2019) Non-Linear Regression Analysis for the Adsorption Kinetics and Equilibrium Isotherm of Phenacetin onto Activated Carbons. *Current Journal of Applied Science and Technology*, **36**, 1-18. https://doi.org/10.9734/cjast/2019/v36i430246

[44] Asuquo, E.D. and Martin, A.D. (2016) Sorption of Cadmium(II) Ion from Aqueous Solution onto Sweet Potato (*Ipomoea batatas* L.) Peel Adsorbent: Characterization, Kinetic and Isotherm Studies. *Journal of Environmental Chemical Engineering*, **4**, 4207-4228. https://doi.org/10.1016/j.jece.2016.09.024

[45] Lekene, N.R.B., Kouotou, D., Ankoro, N.O., Kouoh, S.A.P.M., Ndi, J.N. and Ketcha, J.M. (2021) Development and Tailoring of Amino-Functionalized Activated Carbon Based *Cucumerupsi manni* Naudin Seed Shells for the Removal of Nitrate Ions from Aqueous Solution. *Journal of Saudi Chemical Society*, **25**, Article ID: 101316. https://doi.org/10.1016/j.jscs.2021.101316

[46] Tabi, G.A., Blaise, L.N.R., Daouda, K., *et al.* (2021) Non-Linear Modelling of the Adsorption of Indigo Carmine Dye from Wastewater onto Characterized Activated Carbon/Volcanic Ash Composite. *Arabian Journal of Chemistry*, **15**, Article ID: 103515.

[47] Rezaei Kalantary, R., Dehghanifard, E., Mohseni-Bandpi, A., Rezaei, L., Esrafili, A., Kakavandi, B. and Azari, A. (2016) Nitrate Adsorption by Synthetic Activated Carbon Magnetic Nanoparticles: Kinetics, Isotherms and Thermodynamic Studies. *Desalination and Water Treatment*, **57**, 16445-16455. https://doi.org/10.1080/19443994.2015.1079251

[48] Tran, H.N., You, S.-J., Hosseini-Bandegharaei, A. and Chao, H.-P. (2017) Mistakes and Inconsistencies Regarding Adsorption of Contaminants from Aqueous Solutions: A Critical Review. *Water Research*, **120**, 88-116. https://doi.org/10.1016/j.watres.2017.04.014

[49] Raveendran, K., Anuradda, G. and Kartic, C.K. (1995) Influence of Mineral Matter on Biomass Pyrolysis Characteristics. *Fuel*, **74**, 1812-1822. https://doi.org/10.1016/0016-2361(95)80013-8

[50] Lekene, N.R.B., Kouoh, S.P.M.A., Ndi, N.J., Kouotou, D., Belibi, P.D.B. and Ketcha, M.J. (2015) Kinetics and Equilibrium Studies of the Adsorption of Phenol and Methylene Blue onto Cola Nut Shell Based Activated Carbon. *International Journal of Current Research and Review*, **7**, 1-9.

[51] Abbasi, S. and Hasanpour, M. (2016) The Effect of pH on the Photocatalytic Degradation of Methyl Orange Using Decorated ZnO Nanoparticles with $SnO_2$ Nanoparticles. *Journal of Materials Science: Materials in Electronics*, **28**, 1307-1314. https://doi.org/10.1007/s10854-016-5660-5

[52] Abbasi, S. and Hasanpour, M. (2017) Variation of the Photocatalytic Performance of Decorated MWCNTs (MWCNTs-ZnO) with pH for Photo Degradation of Methyl Orange. *Journal of Materials Science: Materials in Electronics*, **28**, 11846-11855. https://doi.org/10.1007/s10854-017-6992-5

[53] Abbasi, S. (2020) Response Surface Methodology for Photo Degradation of Methyl Orange Using Magnetic Nanocomposites Containing Zinc Oxide. *Journal of Cluster Science*, **32**, 805-812. https://doi.org/10.1007/s10876-020-01847-y

[54] Abbasi, S. (2021) Prediction of Pollutant Removal from Aqueous Solutions Using Magnetic Photocatalysts. *Applied Water Science*, **13**, 1-10.

[55] Abbasi, S. (2021) The Degradation Rate Study of Methyl Orange Using MWCNTs@ $TiO_2$ as Photocatalyst, Application of Statistical Analysis Based on Fisher's F Distribution. *Journal of Cluster Science*, **33**, 593-602. https://doi.org/10.1007/s10876-021-01991-z

[56] Hayeeyea, F., Sattar, M., Chinpa, W. and Sirichote, O. (2016) Kinetics and Thermodynamics of Rhodamine B Adsorption by Gelatin/Activated Carbon Composite Beads. *Colloids and Surfaces A: Physicochemical and Engineering Aspects*, **513**, 259-266. https://doi.org/10.1016/j.colsurfa.2016.10.052

[57] Lee, L.Z. and Zaini, M.A.A. (2020) One-Step $ZnCl_2$/$FeCl_3$ Composites Preparation of Magnetic Activated Carbon for Effective Adsorption of Rhodamine B Dye. *Toxin Reviews*, **41**, 64-81. https://doi.org/10.1080/15569543.2020.1837172

[58] Hoang, L.P., Van, H.T., Nguyen, T.T.H., Nguyen, V.Q. and Thang, P.Q. (2020) Coconut Shell Activated Carbon/CoFe$_2$O$_4$ Composite for the Removal of Rhodamine B from Aqueous Solution. *Journal of Chemistry*, **2020**, Article ID: 9187960.
https://doi.org/10.1155/2020/9187960

[59] Anfar, Z., Zbair, M., Ahsaine, H.A., Ezahri, M. and El Alem, N. (2018) Well-Designed WO$_3$/Activated Carbon Composite for Rhodamine B Removal: Synthesis, Characterization, and Modeling Using Response Surface Methodology. *Fullerenes, Nanotubes and Carbon Nanostructures*, **26**, 389-397.
https://doi.org/10.1080/1536383X.2018.1440386